Continuum Radiation from Active Galactic Nuclei: A Statistical Study.

Takashi Isobe[1] and Eric D. Feigelson[1,2],

Kulinder P. Singh[3,4],

AND

Ajit Kembhavi[4].

Received _____ ; accepted _____

1. Department of Astronomy, The Pennsylvania State University.

2. NSF Presidential Young Investigator.

3. Danish Space Research Institute.

4. Tata Institute of Fundamental Research.

ABSTRACT

The main purpose of this study is to gain insight into physics of the continuum spectrum of active galactic nuclei (AGNs) using a large data set and rigorous statistical methods. We have constructed a database for 469 objects which include radio selected quasars, optically selected quasars, X-ray selected AGNs, BL Lac objects and optically unidentified compact radio sources. Each object has measurements of its radio, optical, X-ray core continuum luminosity, though many of them are upper limits. Since many radio sources have extended components, we carefully select out the core component from the total radio luminosity. With 'survival analysis' statistical methods, which can treat upper limits correctly, these data can yield better statistical results than those previously obtained.

A variety of statistical tests are preformed, such as the comparison of the luminosity functions in different subsmples, and linear regressions of luminosities in different bands. Interpretation of the results leads to the following tentative conclusions: (1) The main emission mechanism of optically selected quasars and X-ray selected AGNs is thermal, while that of BL Lac objects is synchrotron; (2) radio selected quasars may have two different emission mechanisms in the X-ray band; (3) BL Lac objects appear to be special cases of the radio selected quasars; (4) some compact radio sources show the possibility of SSC in the optical band; and (5) the spectral index between the optical and the X-ray bands depends on the optical luminosity.

I. INTRODUCTION

One of the most important problems in the studies of active galactic nuclei (AGNs) is understanding the mechanisms of underlying continuum emission. Although there are already very many observations of AGNs across the whole range of spectrum, and the knowledge of properties of AGNs has been improving considerably, we still do not understand the fundamental emission mechanisms. The continuum emission spectrum distributions probably arise from combinations of several mechanisms, including both thermal and non-thermal processes. The radio emission is thought to be incoherent synchrotron radiation. For some objects like BL Lac objects, the synchrotron spectrum clearly extends to optical region and perhaps to the X-ray band. On the other hand, most of optically selected quasars do not show radio emission and have unpolarized continua. The infrared to ultraviolet regions often have spectral bumps that are not well understood. The emission mechanisms may be combinations of unpolarized synchrotron, bremsstrahlung from an accretion disk, dust emission, stellar photospheric emission, or Compton scattering by thermal or non-thermal electrons. In the X-ray band, synchrotron self-Compton (SSC) is one of the more popular models, though multi-temperature bremsstruhlung is also probable.

Since the *Einstein Observatory* has provided high quality X-ray observations, statistical studies of AGN continua are flourishing (Ku, Helfand, and Lucy 1980; Zamorani *et al.* 1981; Owen, Helfand, and Spngler 1981; Owen and Puschell 1982; Kriss and Canizares 1982; Reichert *et. al.* 1982; Zamorani 1982; Avni and Tananbaum 1982; Blumenthal, Keel, and Miller 1982; Kembhavi and Fabian 1982; Schwartz and Ku 1983; Ledden and O'Dell 1983; Tananbaum, Wandle, and Zamorani 1983; Katgert, Thuan, and Windhorst 1983;

Marshall *et al.* 1983; Bregman 1984; Maccacaro *et al.* 1984; Henriksen, Marshall, and Mushotzky 1984; Cruz-Gonzales and Huchra 1984; Miller 1984; Marshall *et al.* 1984; Ledden and O'Dell 1985; Kriss and Canizares 1985; Stocke *et al.* 1985; Franceschini, Gioia, and Maccacaro 1986). Considerable attention has been focused on the evaluation and interpretation of the average optical-to-X-ray spectral index, $<\alpha_{ox}>$, for various samples of AGNs. These finding are briefly summarized in Table 1. The $<\alpha_{ox}>$ values have been used, for example, to infer that radio-selected quasars are several times more X-ray luminous than optically selected quasars (Ku, Helfand, and Lucy 1980, Zamorani *et al.* 1981), that the broad band spectral index evolves with redshift in radio-quiet quasars (Ku, Helfand, and Lucy 1980, Zamorani *et al.* 1981), and that high polarization quasars and BL Lac objects have similar continuum shapes (Ledden and O'Dell 1985).

In addition to the comparison of broad and spectral indices, statistical correlations between radio, optical, and X-ray emissions in AGNs have also been studied by the previous workers. Ku, Helfand, and Lucy (1980) show a general correlation between radio and X-ray emissions in quasars, which was confirmed and refined in our examination of radio-loud quasars (Kembhavi, Feigelson, and Singh 1986; hereafter Paper II). The close correlation between optical and X-ray luminosities in Seyferts and quasars has been established by a number of workers (e.g. Reichert *et al.* 1982, Blumenthal, Keel, and Miller 1982, Kriss and Canizares 1983, Kriss and Canizares 1985). Zamorani (1984) and Avni and Tananbaum (1986) have examined the relations between the spectral index α_{ox} and optical luminosity and redshift, and Zamorani (1984) has raised the possibility that the quasars X-ray luminosities are simultaneously correlated with their radio and optical luminosities.

Some researchers have expressed a reluctance to examine directly the correlations between luminosities at different spectral bands for fear of encountering spurious correlations, as all luminosities for a given object are scaled by the same $(distance)^2$ factor. We have shown, however, that no such distance-dependent effect occurs if all objects are considered, including those not detected (Feigelson and Berg 1983 and Paper II). A major reason this study has been undertaken is that powerful and well-established statistical techniques are now available that fully account for the presence of upper limits in luminosity-luminosity diagrams (Feigelson and Nelson 1985, Isobe, Feigelson, and Nelson 1986).

The present study represents an improvement upon previous studies in three respects. First, following Paper II, we take particular care to consider CORE radio emission rather than TOTAL radio emission from each AGNs. The total radio flux frequently includes jets and lobes, which does not reflect the current state of activity in the nucleus. While this distinction is small for some classes of AGNs (e.g. radio selected BL Lac objects), it is a considerable correction for others (e.g. 3C and 4C quasars). Note that our earlier VLA observations (Feigelson, Isobe, and Kembhavi 1984; hereafter Paper I) were specifically designed to acquire radio core fluxes for this study. Radio observations from certain optically selected quasars not presented in Paper I, are now presented in § II. Second, we analyze a much larger number of objects than earlier studies by virtue of having collected most or all of the extant literature. The database (§ III) includes all AGNs (except for certain classes, such as Seyfert galaxies and radio galaxies, where the data suffer significant ambiguities) for which radio core, optical and X-ray observations have been reported. All upper limits are included. Third, we use the wide variety of statistical methods provided by 'survival analysis',

the field of applied statistics developed over several decades to solve problems involving upper limits in medical and industrial situations. These methods are reviewed in § IV; the reader is encouraged to examine Feigelson and Nelson (1985) and Isobe, Feigelson, and Nelson (1986) for more details. Applying these statistical methods to the database in § III, we calculate the correlations and linear regressions between X-ray, optical, and radio luminosities. We also investigate several specific issues: (1) The dependence of optical to X-ray spectral index on the optical luminosity and the redshift; (2) a proposed two-component model for X-ray emission of the radio selected quasars; (3) a comparison of the BL Lac objects with the radio selected quasars; and (4) a comparison of the optically selected quasars with the X-ray selected AGNs. The results from these investigation and their interpretations are presented in § V. § VI summarizes the whole study.

II. RADIO OBSERVATIONS

Although most of the data are drawn from the published literatures, we have made two sets of observations with the NRAO[1] *Very Large Array* (VLA) to improve the quality of radio data on certain AGNs with measured X-ray luminosities.

---

[1] The National Radio Astronomy Observatory is operated by Associated Universities, Inc., under contract with the National Science Foundation.

On 23-24 October 1982, thirty-six optically selected quasars with X-ray properties measured by Ku, Helfand, and Lucy (1980), or Zamorani *et al.* (1981) were observed at the VLA. These radio quiet quasars were observed at the same time as the radio loud quasars discussed in Paper I. The array was in the standard B configuration and 26 antennas were operating. The results are given in Table 2a. Twenty-eight quasars were not detected with 5 x rms upper limits around 1 mJy, and 8 quasars were detected with flux densities between 0.8 and 40.5 mJy. Of these, four were not (to our knowledge) previously known radio sources, including the comparatively bright quasars GQ Com and V396 Her.

In the second set of VLA observations, we observed the X-ray selected AGNs from the serendipitous *Einstien* IPC sample of Kriss and Canizares (1982). The observations were performed along with the survey of discussed by Gioia *et al.* (1984) on 28-30 November 1981 with the VLA in the C configuration. The results are given in Table 2b. Data for one object in the sample, 0514-003, were not good. Snapshots of ~12 minutes duration gave 5 x rms upper limits around 0.7 mJy for 21 of the sources. Three are detected, one of which (1401+085, z=0.43, S_5=18.8 mJy) is quite radio luminous.

III. DATABASE

This study is base on the radio, optical and X-ray luminosities of a variety of AGNs given in Tables 3, 4, and 5. In Table 3, we show data on the radio selected, optically selected, and X-ray selected samples of emission line AGNs. Data on BL Lacertae type objects are shown in Tables 4a and 4b. Table 5 includes optically faint or undetected AGNs for which redshifts measurements are not available.

The database, however, excludes certain classes of AGNs for which unambiguous radio cores, optical magnitudes or X-ray data are not available. Few Seyfert galaxies have optical core magnitudes reported separately from the host galaxy brightness, and their radio structures are frequently complex so that the core is not readily discriminated from ejecta (e.g. Ulvestad and Wilson 1983). Radio galaxy nucleus X-ray emission may be often confused by the diffuse X-ray of the surrounding intercluster medium (Feigelson and Berg 1983), and again optical core magnitudes are usually not available. The PG sample of bright optically selected quasars (Schmitt and Green 1986, Tananbaum *et al.* 1986), the Braccesi and other fields of faint optically selected quasars (Braccesi *et al.* 1970, Marshall *et al.* 1984) have X-ray observations, but sensitive radio measurements have yet to be published. All of these samples have therefore been omitted from our study.

Data in Tables 3 and 4 are organized as follows: Column 1 lists the source by its Right Ascension and Declination. Column 2 gives the catalog name from the various radio and optical surveys. Column 3 gives the redshift values taken from the X-ray literature, if available, or from other sources described in the Notes to Tables 3 and 4. In column 4, we give the radio core luminosities for the sources. The luminosities are computed using the

following formula:

$$\ell = 4\pi\, d_\ell^2\, f\, (1+z)^{(\alpha-1)},$$

where α is the spectral index within the appropriate spectral band ($f \sim \nu^{-\alpha}$), and f is the observed flux density, z is the redshift and d_ℓ is the luminosity distance given by

$$d_\ell = \frac{cz}{H_0}\,(1+\frac{1+z}{2}),$$

where we assume a Hubble constant $H_0 = 50$ Mpc/km/sec and $q_0 = 0$. For the radio core emission, we assume the spectral index within the radio band, $\alpha_r = 0$. Since many radio selected quasars have extended components, we use the following procedure to find the core luminosity density at 5 GHz:

i) If a map that clearly resolves the core from any jets or lobes is available, the core flux density is used. If the map is not at 5 GHz, the core spectral index is assumed to be 0.0.

ii) If the source is fully resolved and the core is not detected, we use an upper limit given in the literature. If an upper limit is not given, the flux density of the weakest component is used as an upper limit.

iii) If an interferometric map is not available, but the source is seen by single dishes and the spectral index between 1.4 GHz and 5 GHz is less than 0.3, the entire flux density given for the object is assumed to be the core flux density.

iv) If single dish data are available, and the spectral index is steeper than 0.3, the 5 GHz flux density given for the object is treated as an upper limit, even if it is detected. This is because of the probable existence of extended components. Although a distribution of the upper limits set by this procedure may not be same as that of the upper limits due to the flux limited observation, we assume that all upper limits belong to a same population. As discussed in Paper II, even such careful efforts to isolate radio core fluxes

can leave a residual ~ 50% extra flux from VLBI scale jets.

The majority of optically selected quasars and X-ray selected AGNs are not detected in the radio band. Those that are detected are generally faint and unresolved, and their flux is assumed to arise from a core with α_r=0.0. Cases where the radio measurement, either detection or upper limit, was made at 2.7 GHz or 1.4 GHz rather than 5 GHz are marked by a * or + in Table 3.

The optical luminosities are given in column 5. For optical emission, the spectral index within the optical band, α_o=1.0, is assumed. Visual magnitudes are mainly taken from Hewitt and Burbidge (1980). The visual magnitudes are converted to the optical luminosity density at 2500 Å according to Zamorani *et al.* (1981),

$$\log(\ell_o)=37.878 + 2\cdot\log[z(1+\frac{z}{2})] - 0.4V_{corr} + \frac{0.072}{sin(b)},$$

where V_{corr} is the visual magnitude corrected for MgII line emission (Schmidt 1968), and the last term is a correction for galactic absorption, where b is the galactic latitude. If only a blue magnitude is available, the equation is modified as

$$\log(\ell_o)=38.011 + 2\cdot\log[z(1+\frac{z}{2})] - 0.4B_{corr} + \frac{0.072}{sin(b)},$$

where B_{corr} is the corrected blue magnitude from Schmidt. If a redshift is not available, an optical flux density at 2500 Å at the observer's frame is computed to find α_{ro} and α_{ox},

$$\log(f_o)=-19.756 - 0.4V + \frac{0.072}{sin(b)}.$$

For some compact radio objects, since only red magnitudes are available, we need to change the constant in the last equation to -19.521 (Johnson 1966).

Column 6 lists the X-ray luminosities computed for the 0.5-4.5 keV energy range in the emitting frame and assuming the spectral index within the X-ray band α_x =0.5. The X-ray data are obtained mostly from the observations with the *Einstein Observatory*, although some data from observations with the HERO-1

satellite are also included. If the X-ray luminosity in the above energy band already exists, then it is adopted directly, else it is calculated from the observed flux in the 0.5-4.5 keV energy band according to the fomulae given after Table 5. Column 7 lists the radio spectral index of the core wherever the measurement exists.

The values for the spectral index (α_{ro}) computed between the radio (5 GHz) and the optical (2500 Å) bands in the emitting frame are listed in column 8. These values are calculated using the following expression:

$$\alpha_{ro}=(\log\ell_r - \log\ell_o)/5.38.$$

If the redshifts are not available, we use the flux densities instead of the luminosities. The spectral index (α_{ox}) between 2500 Å and 2 keV emission is given by

$$\alpha_{ox}=(\log\ell_o - \log\ell_x - 17.98)/2.61.$$

The values for α_{ox} are listed in column 9. Column 10, 11, and 12 list the references for the radio, optical, and X-ray data respectively.

Although not shown as separate tables, a few other subsamples are used. For some statistical problems, we use spatially resolved radio selected quasars, unresolved radio selected quasars with flat ($\alpha_r<0.3$), and steep ($\alpha_r>0.3$) spectra. These samples are discussed in detail in Paper II.

Comparison of our data calculated luminosities, α_{ro} and α_{ox} values to previous collection of continuum emission in AGNs, such as Ku, Helfand, and Lucy (1980), Zamorani *et al.* (1981), and Ledden and O'Dell (1985), shows relatively good agreement. One relatively large discrepancy is the radio luminosity, since we use the core instead of the total luminosities. The difference in the radio luminosities often reachs an order of magnitude difference. Because of this, the spectral index between the radio and optical band can show relatively large discrepancies. In addition, the BL Lac objects

often show large differences from other studies. This may be due to their high degree of variability.

There are several possible sources of error in the database. First, data are collected from variety of references and may be differently treated in each reference. Second, and related to the first point, uncertainty arises when a source is variable and observations are not done simultaneously. Third, some error is caused by the extrapolation of published data with fixed spectral indices to compute luminosity densities at consistent wavelength in the emitting frame. For example, this may be an important error source for the optical luminosity density, since we do not consider the effect of 3000 Å bump and other effects in UV region. Fourth, although we use point radio sources in VLA maps as cores, VLBI observations often show that the cores can be resolved to further small scale. Therefore, the core radio luminosity density may be systematically overestimated. Some small errors also arise from assuming a specific cosmology. Although the Hubble constant H_0 does not affect correlations, the cosmological constant q_0 does.

Based on comparisons of luminosities with previous studies and our estimation of the size of these possible sources of error, we find typical 1σ uncertainties of ± 0.2 in $\log(\ell_r)$, $\log(\ell_o)$, and $\log(\ell_x)$. Although these error sources may seem large, uncertainties of less than 0.5 in log form are not very significant, since the ranges of ℓ_r, ℓ_o, and ℓ_x are frequently 10^6.

IV. STATISTICAL METHODS

Since the data set contains many upper limits, survival analysis must be used to treat the data correctly. Survival analysis or the analysis of lifetime data, is developed over several decades to deal with problems arises in clinical epidemiology, actuarial science and industrial reliability, where 'censored data' (i.e. upper or lower limits) frequently arise. The methods are typically extensions of parametric (e.g. least square regression) or non-parametric (e.g. Kolmogorov-Smirnov or Mann-Whitney tests) statistical tools used for uncensored data, and frequently involve maximum-likelihood concepts. Most of the procedures we use in this study are described by Feigelson and Nelson (1985) and Isobe, Feigelson, and Nelson (1986). The former study treats problems involving one variable: the Kaplan-Meier estimator is the maximum-likelihood estimator of the luminosity and gives a mean luminosity and a standard deviation for a sample; the Gehan and logrank tests measure whether two subsamples are drawn from a same parent population. The latter study treats correlation and regression between two variables: Cox regression and the generalized Kendall's τ test (the BHK method) which measure the degree of independence; the EM algorithm and Buckley-James methods perform linear regression on the data.

One new method is used in this study. Previously, we could not fit a line on a data set which contains upper (or lower) limits in both independent and dependent variables, except by Schmitt's (1985) method which does not provide analytic estimates of the uncertainties for the regression parameters. Using the BHK method described by Isobe, Feigelson, and Nelson (1986), we have developed a method to find a slope coefficient and uncertainty. Consider a database in two variables (X_i, Y_i) with possible non-detections in both

variables. For a range of slope coefficients b, calculate residuals $r_i=Y_i-bX_i$. The value of b that minimizes the generalized Kendall's τ rank correlation coefficient between the r and X is the most probable value. The 1σ uncertainties can be obtained by finding the slope coefficients which give 31% of the maximum probability. To find the intercept coefficient, we use the Kaplan-Meier estimator. First, get the residuals r with the best slope coefficient b. The best estimate of the intercept coefficient is the Kaplan-Meier mean of the residuals. This combination of survival analysis methods on doubly censored data may permit parameter estimation for non-linear models as well. We use it in § IV to test a two-component model of quasar X-ray emission. Although similar procedures have been already suggested for non-censored data sets by statisticians (Sen 1968, Efron 1984, Lancaster and Quade 1985), there is no statistical study for censored data sets yet. From our experience, however, the resulting regression coefficients are quite satisfactory when compared to those obtained by other methods.

Using these survival analysis techniques, we analyze our database. Cox regression and the BHK method are used to compute the correlation probabilities between the radio, optical, and X-ray luminosities, and the EM algorithm and Buckley-James method (and the new linear regression method, if needed) are used to calculate the linear regression coefficients (§ V*a*). The mean values of the spectral indices are calculated by Kaplan-Meier estimator (§ V*b*). Multi-dimensional linear regression among the optical luminosity, the redshift, and the spectral index between the optical and the X-ray bands is discussed in § V*c*. The new regression method is applied to analyze the two-component model for the X-ray emission of the radio selected quasars (§ V*c*). For the comparison of the BL Lac objects and the radio selected quasars, and the comparison of the optically selected and the X-ray selected AGNs, the two

sample tests (Gehan and logrank tests) are used (§ V*e*,*f*).

V. STATISTICAL ANALYSIS AND INTERPRETATION

We now proceed to investigate a number of statistical relations between the ℓ_r, ℓ_o, and ℓ_x values listed for the various samples in Tables 3 to 5. Most of the relationships are illustrated in Figures 1 to 3, which plot the luminosity densities against each other, and Figure 4, which plots the interband spectral indices α_{ox} vs. α_{ro}. The plots are displayed so that the various subsamples can be easily distinguished.

All data lie in the range of $29 < \log(\ell_r) < 37$, $28 < \log(\ell_o) < 33$, $42 < \log(\ell_x) < 48$, $-0.3 < \alpha_{ro} < 1.2$, and $0.8 < \alpha_{ox} < 1.9$. The radio quasars tend to occupy higher and relatively wider range (six decades for radio, four decades for optical and X-ray). BL Lac objects occupy similar range as the radio quasars. The optically selected quasars are usually one order of magnitude weaker than the radio quasars. The X-ray selected AGNs occupy same range as the optically selected quasars do. The X-ray selected BL Lac objects are few in number and occupy only two decades in any luminosity; hence we will not be surprised if significant statistical results are not obtained.

a) Correlations and Linear Regressions between AGN Luminosities

Using Cox regression and the BHK method, we establish the significance level of correlations between radio and X-ray luminosities, optical and X-ray luminosities, optical and radio luminosities, and α_{ro} and α_{ox} for all subsamples described in § III. Quantitative results are shown in Table 6a. The first column lists the name of the samples and the second column lists the correlations tested. The third column shows the total number of the objects and the fourth column lists the number of censored data. Three values are the

numbers of data points which are censored in the independent variable only, the dependent variable only, and both the variables, respectively. The fifth and sixth columns show the correlation probabilities by Cox regression and the BHK method; This is the probabilities that the two variables are not correlated with each other. The last column identifies the corresponding figure. Except for some spectral index correlations, all subsamples show high significant level between all spectral bands. For example, even the optically selected quasars show a highly significant correlation ($P<0.01\%$) for the radio and X-ray luminosity relation.

Although we find very high significant levels for nearly all correlations, it is difficult to tell which correlations are intrinsic and which correlations are secondary. For a completely detected data set, we can use a partial linear correlation method and a partial rank correlation, but these methods cannot treat a censored data set. Using the generalized Kendall's τ correlation coefficient, we may be allowed to use a normal partial rank correlation formula, but since a partial rank correlation is distribution free, we cannot get significant levels. We show the partial correlation coefficients results shown in Table 7, but they can be used only for qualitative examintion.

For the radio selected quasars, the optical / X-ray relation is most significant ($r=0.45$, where r is the partial correlation coefficient in Table 7) and the radio / X-ray relation is also important ($r=0.42$), but the optical / radio relation may not be significant ($r=0.13$). For the optically selected quasars and the X-ray selected AGNs, the optical / X-ray relation is most important and two other relations may not be significant. For the radio selected BL Lac objects, the radio / X-ray relation is most significant and the optical / X-ray relation is moderately significant, but the optical /

radio relation is weaker. For the X-ray selected BL Lac objects, the optical / X-ray relation is most important, and the optical / radio relation is moderately important, though because of small size of the data, this finding may not be accurate. We thus find that the ℓ_o / ℓ_x relations are typically of greatest importance, with the ℓ_r / ℓ_x and ℓ_r / ℓ_o relations important only in certain subsamples.

The linear regressions are done mainly by the EM algorithm which assumes the luminosities are distributed in a Gaussian distribution about the best fit line, and the Bukley-James method, which makes no assumptions regarding the distribution of residuals. Since the relation between $\log(\ell_r)$ and $\log(\ell_x)$ contains upper limits in both variables in the same subsamples, the new method described in § IV is used to compute coefficients. Quantitative results are shown in Table 6b. The first column lists the name of the samples and the second column lists the independent and the dependent variables. The third column shows the total number of the objects and the forth column lists the number of censored data. The fifth and sixth columns show the linear regression results by the EM algorithm and Buckley-James method respectively. The first row in the each set shows the intercept coefficient, the second row shows the slope coefficient, and the last row shows the standard deviation. If only one set of the result appears, the regression was done by the new method described in the § IV, or by a normal least square method, if there are no censored data. For example, the radio selected quasars have the linear regression form, $\log(\ell_x)=29.0+(0.48\pm0.06)\log(\ell_r)$. This best fit line is shown in Figure 1*a*.

The linear regressions can be summarized as follows. The radio/X-ray correlation is about $\ell_x \propto \ell_r^{0.5}$ for quasars of all types but is significantly steeper ($\ell_x \propto \ell_r^{0.8}$) for BL Lac objects. The optical/X-ray correlation behaves

similarly ($\ell_x \propto \ell_o^{0.7}$ for quasars compared to $\ell_x \propto \ell_o^{1.0}$ for BL Lacs), though the X-ray selected AGN subsample does not fit the pattern. The radio/optical correlation is $\ell_r \propto \ell_o^{1.0}$ for the radio and the optical quasars as well as the BL Lac objects, but, as stated above, may be an indirect consequence of the ℓ_r/ℓ_x and ℓ_o/ℓ_x correlations. The correlation is present in X-ray selected AGNs and the X-ray selected BL Lac objects, but they have very different forms from the others.

A plausible theoretical interpretation of these results might be as follow. First, the results of partial correlation analysis (strong correlation between ℓ_o and ℓ_x but not between ℓ_r and ℓ_x) suggest that for the optically selected quasars and the X-ray selected AGNs, the thermal emission (e.g. bremsstrahlung, Comptonization) is the dominant mechanism. The thermal emission scale according to $\ell_x \propto \ell_o^{(0.7\pm0.1)}$. This form is predicted by Tucker (1983) and Schlosman, Shaham, and Shaviv (1984) for the thermal emission from accretion disks. Second, for the BL Lac objects, because of the strong correlation between ℓ_r and ℓ_x, non-thermal emission is most important. The non-thermal emission may have the form of $\ell_x \propto \ell_r^{(0.8\pm0.1)}$. Third, for the radio selected quasars, the X-ray emission depends on both the radio and optical emissions. The result indicates that there are possibly two different X-ray emission mechanisms (see § V*d* for the further disccusion).

b) Mean Values of the Spectral Indices

The relation between the interband spectral indices are shown in Figures 4*a* to 4*e* with quantitative results given in Table 8. All mean values and standard deviations were calculated using the Kaplan-Meier estimator (§ IV). As expected from simple selection effects, $\langle \alpha_{ro} \rangle$ is relatively large in the

radio selected quasars and BL Lac objects, and $<\alpha_{ox}>$ is relatively large in the optically selected quasars. All subsamples except the compact radio sources show $<\alpha_{ro}> \sim 0.5$ and $<\alpha_{ox}> > 1.0$. On the other hand, the compact radio sources show $<\alpha_{ro}> \sim <\alpha_{ox}> \sim 1.0$. This means that one power law with $\alpha \sim 1.0$ can express the entire emission between the radio and X-ray bands for this subsample. Close examination of Table 5 also tells that some objects may have $<\alpha_{ro}> > <\alpha_{ox}>$. Since this relation cannot be readily produced by thermal or the synchrotron processes, this may be direct evidence for the SSC model operating in the optical to X-ray bands.

In Table 1, we summarized published values α_{ox} and α_{ro} from recent literature. A comparison with our results shows that although they are not exactly the same as our values, they agree reasonably well. For the BL Lac objects, our results are very similar to Ledden and O'Dell's (1985) results because of the similar database. We note, however, substantial differences among different studies of optically selected quasars, ranging from $<\alpha_{ox}>=1.37 \pm 0.10$ (Marshall *et al.* 1983) to $<\alpha_{ox}>=1.65 \pm 0.03$ (this study). Since Marshall *et al.* treat lower luminosity objects, this may cause the difference as we can see in an other study (Zamorani *et al.* (1981) find for radio quiet quasars that $\alpha_{ox}=1.37+0.05/-0.08$ for $\log(\ell_o)<31.4$ but $\alpha_{ox}=1.62+0.08/-0.11$ for $\log(\ell_o)>31.4$). Other possible causes for discrepances are the use of different optical magnitudes (i.e. not those of Hewitt and Burbidge 1980), frequences at each band (Owen, Helfand, and Spangler 1981, Cruz-Gonzales and Huchra 1984), selection criteria (Zamorani *et al.* 1981), correction factors for absorption and MgII line (Margon, Downes, and Chanan 1985), and different spectral indices assumed for extrapolations.

c) Luminosity Ratio Dependence on Optical Luminosity and Redshift

The dependence of α_{ox} on optical luminosity and/or redshift for the optically selected quasars is often discussed (Reichert *et al.* 1982, Avni and Tananbaum 1982, Zamorani 1982, Maccacaro and Gioia 1983, Zamorani 1984, Kriss and Canizares 1985, Avni and Tananbaum 1986). Avni and Tananbaum (1982) were the first to obtain a relation among them using survival analysis (the "detection-and-bounds" linear regression method, see Avni and Tananbaum 1986). Their relation is expressed as

$$\alpha_{ox}=(-0.0\pm0.3)(\tau-0.5)+(0.12\pm0.06)[\log(\ell_o)-30.5]+1.50,$$

where $\tau = z/(1+z)$. They mention that explicit dependence of α_{ox} on the optical luminosity is predominant, but the joint dependence of α_{ox} on both variables is possible. This result is confirmed in a more recent paper (Avni and Tananbaum 1986).

Zamorani (1982) shows a similar relation for a combined sample of optically selected quasars and Seyfert galaxies. Ignoring the dependence on the redshift, Zamorani (1984) finds

$$\alpha_{ox}=0.129\ \log(\ell_o)-2.427.$$

In another subsample, Tanambaum, Wandle, and Zamorani (1983) find a similar relation for radio selected quasars (the 3CR sample),

$$\log(\ell_x)=27.63+(0.47\pm0.15)[\log(\ell_o)-31.20]+(0.14\pm0.12)[\log(\ell_r)-34.78]$$
$$-(0.45\pm0.78)[\log(1+z)-0.26].$$

Because of the weak dependence on the radio luminosity and the redshift, they rewrite this relation as

$$\alpha_{ox}=0.20\ \log(\ell_o)-4.98.$$

We look for analogous relations in our data sets; the results are shown in Tables 9a and 9b. In Table 9a, we show the relations between α_{ox} and τ and

between α_{ox} and log (ℓ_o). Assumed regression forms are $\alpha_{ox}=a+b\tau$ and $\alpha_{ox}=a+b\log(\ell_o)$. We find the $\log(\ell_o)$ - α_{ox} slope to be 0.11 ±0.02 for radio selected and optically selected quasars. Only the optically selected quasars show high significance levels for both the redshifts and the optical luminosity regressions. These relations, however, might be artificial, since for the optically selected quasars, the optical luminosity is biased due to optical magnitude limited survey. The direction of evolution of the optically selected quasars agrees with the results by Ku, Helfand, and Lucy (1980) and Zamorani *et al.* (1981) (see Table 1).

We also compute the three dimensional regressions for α_{ox}, τ, and $\log(\ell_o)$, using the regression form of Avni and Tananbaum (1982). The results are shown in Table 9b. The second column shows Cox probabilities. The first value is a joint probability that no correlation exists between α_{ox} and both redshift and $\log(\ell_o)$, the second value is the probability for the redshift alone, and the third is for optical luminosity density alone. The second and third values are determined assuming the ratio of the slope coefficient and the error is distributed as a Gaussian. The third column shows the regression results. All subsamples, except the X-ray selected BL Lac objects (P=23%), show highly significant joint probabilities ($P \leq 0.01\%$). Only the optically selected quasar sample does not show significant correlations for the individual variables (P(z)=53% and P(ℓ_o)=42%), even though this subsample is the only one which shows high significance levels for correlation between α_{ox} and τ, and α_{ox} and $\log(\ell_o)$. Although this result does not confirm Avni and Tananbaum's result which shows that α_{ox} is positively correlated with $\log(\ell_o)$, we find similar relations (high joint and individual probabilities) in other subsamples.

The interpretation for the radio selected quasars, X-ray selected AGNs, and BL Lac objects is that objects at higher redshifts have higher ℓ_x/ℓ_o ratios, and those with higher optical luminosities have lower ℓ_x/ℓ_o ratios. For example, a typical radio selected quasar at z=2 will have a ℓ_x/ℓ_o ratio twice that of a similar quasar at z=0. At a given redshift, a typical radio selected quasar with $\log(\ell_o)$=32 will have a ℓ_x/ℓ_o ratio half that of a similar quasar with $\log(\ell_o)$=33. The slope coefficients in Table 9b can be used to give analogous results for other subsamples.

We also examine the dependence of α_{ox} on an X-ray luminosity and a redshift. The results are in Table 9c. Because of the presence of censoring in ℓ_x as well as α_{ox}, we can obtain results only for the X-ray selected AGNs and the BL Lac objects. Although the X-ray selected AGNs show a high significance level for both the variables, the BL Lac objects do not.

Comparing these three results, we find some inconsistencies. The radio quasars, X-ray AGNs, and BL Lac objects show weak positive correlations between α_{ox} and r in Table 9a, but strong negative correlations in Table 9b. Table 9c shows another problem. In the relations among α_{ox}, r, and $\log(\ell_x)$, the direction of the dependence on r is opposite to that of r in the relations among α_{ox}, r, and $\log(\ell_o)$. If there is a real dependence of α_{ox} on r, the direction should be the same. These inconsistencies suggest that either α_{ox} does not truly depend on r, or that the evolution is different for the various wavebands and subsamples.

d) Two Component Model for X-ray Emission of the Radio Selected Quasars

Although an important emission mechanism of the radio selected quasars is thought to be the synchrotron radiation, the slope of the $\log(\ell_r)$ - $\log(\ell_x)$ is

much shallower ($\ell_x = \ell_r^{0.48\pm0.06}$) than that of BL Lac objects ($\ell_x = \ell_r^{0.77\pm0.08}$), whose emission mechanism is almost certainly the synchrotron. A close examination of the plot (Fig. 1a) shows that the distribution of data points does not follow a straight line. This has been be interpreted as evidence for two different types of the radio selected quasars (Owen, Helfand, and Spangler 1981, Owen and Puschell 1982, and Zamorani 1984).

Zamorani (1984) has suggested that there are two different X-ray emission mechanisms; for example, a synchrotron component and a thermal component. For the relation between ℓ_r and ℓ_x (see Fig. 1a), the emission mechanism of the steeper component at high luminosities would be mainly non-thermal, and that of the flatter component at lower luminosities would be thermal or a combination of the non-thermal and thermal emission. Since if the X-ray emission is a thermal origin, the X-ray luminosity is expected to be independent from the radio luminosity. This explanation is supported by the partial correlation coefficients studied in the § Va, since the partial rank coefficients between the radio luminosity and the X-ray luminosity and that between the optical luminosity and the X-ray luminosity are equally strong. The X-ray emission related to the radio luminosity may be a synchrotron or SSC radiation because of the similarities to the BL Lac objects, and the emission related to the optical luminosity may be a thermal radiation because of the similarities to the optically selected quasars. Zamorani adopts a three dimensional regression model with a form of

$$\ell_x \propto \ell_o^{b_o} + \ell_r^{b_r}.$$

He finds that for the flat spectrum radio selected quasars, b_o=0.75 and b_r=0.95, and for the steep spectral radio selected quasars, b_o=0.63 and b_r=0.75. Since the survival analysis cannot treat non-linear problems, we adopt Zamorani's b-values. Then, using our data set and the application of

the BHK method, we find his equations can be rewritten as

$$\log(\ell_x)=\log(\ell_o^{0.75}+5\times10^{-10}\ell_r^{0.95})+21.8,$$

$$\log(\ell_x)=\log(\ell_o^{0.63}+3\times10^{-7}\ell_r^{0.75})+26.0,$$

respectively. The model seems to fit well; however, we found that the computation of b-values heavily depends on a few points and hence the value is unstable.

To judge whether this two component model is needed to fit the data, we compare these models to the other simple models. One is a straight line ($\log(\ell_x)=29.0+0.48\log(\ell_r)$) and another consists of two straight lines ($\log(\ell_x)=19.0+0.77\log(\ell_r)$ for $\log(\ell_r)>33.77$ and $\log(\ell_x)=45.0$ for $\log(\ell_r)<33.77$). The last model is made by assuming that the steeper components have the same slope coefficient as the BL Lac objects and the flat components have a zero slope coefficient. The other coefficients are then found using the BHK method. Since we do not have either a χ^2-test or an other goodness-of-fit test to compare models for censored data, we need to use a non-standard method. The Kaplan-Meier estimation of distribution of residuals found by subtracting these models from the data is examined. The 25th and 75th percentiles of the residuals express the dispersion of the data about the model. One problem is that these dispersions cannot be translated to probabilities, and hence the results are only qualitative.

We find dispersions of 0.65, 0.63, 0.51, and 0.44 about the straight line model, the two straight line model, the flat radio spectra model, and the steep radio spectra model respectively. Zamorani's (1984) models are thus better than these other models of the X-ray emission for radio selected quasars.

Additional support for these composite models is presented in Paper II and Kembhavi (1986). In these papers, we compare spatially resolved and

unresolved radio quasars. The subsample of the resolved quasars (with arcsecond resolution) has a shallower slope ($\ell_x \propto \ell_r^{0.35\pm0.04}$) compared to the subsample of the unresolved quasars ($\ell_x \propto \ell_r^{0.71\pm0.07}$ for the unresolved quasars with $\alpha_r<0.3$; see Fig. 3 in Paper II). These results are confirmed in our enlarged data set using survival analysis.

If the X-ray emission mechanism of the resolved radio selected quasars is dominantly thermal, and that of the unresolved radio selected quasars is non-thermal, then we can expect a flat slope for the resolved, and a steep slope for the unresolved radio selected quasars.

e) BL Lac Objects

In our data sets, the radio selected BL Lac objects have a distinct position. Since all the objects are detected in all three frequencies, statistical results are free from the selection effect due to the flux limited observations. Also because of their nonthermal nature (supported by short variabilities, high polarizations, and our partial correlation results), they can be used as a standard to which other subsamples are compared.

Since the BL Lac objects have no upper limits, the partial linear correlation probabilities in Table 7 can be computed to find which relations are significant. The partial linear correlation probabilities are P(rx,o)<0.01%, P(ox,r)=2%, and P(ro,x)=20%, where, for instance, P(ro,x) is the correlation probability between the radio and the optical luminosity for a fixed X-ray luminosity. The results show that the radio/X-ray relation is most significant, and the optical/X-ray relation is moderately significant, but the optical/radio relation is not significant.

Some researchers have pointed out the similarities between the BL Lac objects and the radio selected quasars. Using two sample tests, we compare these subsamples. First, we use all data in both the samples. The results are shown in Table 10a. The optical and the X-ray luminosities of the radio selected quasars are higher than those of the BL Lac objects, which is probably a consequence of the fact that the radio selected quasars have a much wider distribution in the redshift than the BL Lac objects. If the redshift range for both the subsamples is restricted to 0.8 and 1.7, better agreements in the mean luminosities are found (Table 10b). There are, however, some problems. There are only eight BL Lac objects in this restricted sample, and they do not show any internal radio, optical, or X-ray correlations. The radio selected quasars, in contrast, give the slope coefficients 0.34+0.10/-0.08 for $\log(\ell_r)$-$\log(\ell_x)$ and 0.45 ± 0.11 for $\log(\ell_o)$-$\log(\ell_x)$, though no significant relation exists between $\log(\ell_o)$ and $\log(\ell_r)$. These results can be interpreted in two ways. One interpretation is that there are no significant differences in the continuum spectra of radio selected quasars and BL Lac objects, and another is that the data are too fragmentary to give firm conclusions. More BL Lac objects are needed.

The unresolved radio selected quasars are also compared with the BL Lac objects. The samples with restricted redshift range show strong similarities. Therefore the BL Lac objects may be special cases of the radio selected quasars.

The distinctive difference between the radio selected and the X-ray selected BL Lac objects are often noted (Ledden and O'Dell 1985, Stocke *et al.* 1985). For example, the mean spectral indices are: $\langle\alpha_{ro}\rangle$= 0.62 ± 0.02, $\langle\alpha_{ox}\rangle$=1.46 ± 0.03 for the radio selected BL Lac objects, and $\langle\alpha_{ro}\rangle$=0.37 ± 0.02, $\langle\alpha_{ox}\rangle$=1.11 ± 0.04 for the X-ray selected BL Lac objects. Ledden and

O'Dell (1985) suggest that the main emission mechanisms of the X-ray BL Lac objects is the synchrotron radiation, and the radio selected BL Lac objects have extra mechanisms, such as beaming. If we compare the averaged luminosities of the radio selected and the X-ray selected BL Lac objects, we find that the radio selected BL Lac objects are 100 times more luminous than the X-ray selected BL Lac objects in the radio band, 7 times more luminous in the optical band, and nearly same in the X-ray band. This may support the beaming model.

But an alternative possible explanation is a selection effect. In the diagram of α_{ro}/α_{ox} relation, we see that the radio selected and the X-ray selected BL Lac objects mark the lower and upper bounds of the radio selected quasars. The difference between these two groups may be due to two extreme cases of sources with the same emission mechanism as in the radio selected quasars. A similar offset in the $<\alpha_{ro}>$ is seen between the radio selected quasars and the optically selected quasars and the X-ray selected AGNs which can be attributed largely to the selection methods used in their discovery. If so, we may find "optically selected" BL Lac objects somewhere between these two groups. Only one BL Lac object was possibly found optically (ZWI 186), and it is located among the X-ray selected BL Lac objects. Optical surveys for high polarized objects (e.g. Borra and Corriveau 1984) have been generally unsuccessful.

f) Comparison of the Optically Selected Quasars and the X-ray Selected AGNs

It is often mentioned that the optically selected quasars and the X-ray selected AGNs have similar natures, and the latter are treated as a lower luminosity sequence of the former (e.g. Maccacaro *et al.* 1984, Kriss and

Canizares 1985). In our data sets, both subsamples show a strong correlation between the optical and the X-ray luminosities but do not show the other relations (see § Va). This initially suggests that the X-ray and optical emission mechanisms of these subsamples are similar. In the plot of $\log(\ell_o)$ and $\log(\ell_x)$, however, the slope coefficient of the X-ray selected AGNs are significantly steeper (0.87 ± 0.05) than that of the optically selected quasars (0.70 ± 0.06). Also the α_{ox} indices of the X-ray selected AGNs tend to be shallower ($<\alpha_{ox}> = -1.65 \pm 0.03$) than those of the optically selected quasars ($<\alpha_{ox}> = -1.35 \pm 0.02$). The average radio and optical luminosities of the optical selected quasars are about 20 times brighter than those of the X-ray selected AGNs, but the average X-ray luminosity is nearly the same. If the emission mechanism of these two subsamples were the same, the difference of the brightness of each band should be approximately same. One explanation of this difference is suggested by Kriss and Canizares (1985). They show that the high redshift objects are much "redder", since the optical band shifts to shorter wavelength which is strongly affected by reddening, while the X-ray band is not affected much. Hence, if we compare the optically selected quasars which have, on the average, a higher redshift to the X-ray selected AGNs which have, on the average, a lower redshift, then the optically selected quasars show more absorption.

(g) Groping towards the Physics of AGN Continua

Having investigated the relations between the continua of various types of AGNs, we should like to know the relevance of the various models of physical processes of continuum emission to the results of our statistical analyses. There are fundamentally two different mechanisms: a thermal

radiation from an accretion disk, and a non-thermal radiation from the vicinity of the central engine or jets. If the thermal emission from the accretion disk is the main mechanism (Tucker 1983, Schlosman, Shaham, and Shaviv 1984), X-ray and optical luminosities may show a correlation but the radio luminosity is likely to be independent. According to Tucker (1983), the emission from an optically thick accretion disk can generate the relation $\ell_x \propto \ell_o^{\alpha}$ with α=0.5 to 0.8. Most of our results are consistent with this prediction (α~0.7, except for BL Lac objects where $\alpha \sim 0.9$), though the thermal model does not explain the radio/X-ray correlation seen in most samples. If the entire continuum is due to synchrotron emission, the X-ray, optical, and radio luminosities should be well correlated each other with $\alpha_{ox} \geq \alpha_{ro}$. All subsamples agree with these conditions. If the synchrotron self-Compton (SSC) mechanism is important, a strong correlation between the radio and X-ray is expected with a possible correlation with the optical luminosity through the synchrotron emission. If beaming due to a relativistic jet exists, it would lead to correlation between all beamed (presumebly nonthermal) components. Other mechanisms, such as Compton scattering of blackbody or cyclotron radiation could also be responsible for the power low spectrum in the optical to X-ray bands.

These various models clearly do not make predictions which can be uniquely distingushed by the $\ell_r/\ell_o/\ell_x$ database studied here. Most models are not sufficiently developed to predict how radio, optical and X-ray luminosities should scale. Nontheless, we can attempt to reach some crude conclusions. The fact that ℓ_r is correlated with both ℓ_o and ℓ_x in virtually all subsamples of AGNs (Table 5a) is evidence against a thermal model for the continuum spectrum unless, for example, there is some indepedent scaling between the size of the thermal accretion disk and the strength of the non-

thermal jets. The correlation between all three bands is fully consistent with a simple or beamed synchrotron model, though models must account for fact that the scaling between bands is not quite linear (Table 5b). There are no indications that ℓ_r and ℓ_x are correlated with ℓ_o decoupled, as might occur in an SSC model, but this cannot be conclusive evidence against SSC as the optical band could be dominated by non-thermal continuum (e.g. Königl 1981).

Although it is risky to pursue more elaborate models when adjudication between the simplest ones is difficult, we find the two component AGN continuum model discussed in § V*d* is attractive. Here all AGNs have the thermal emission from the accretion disk and the non-thermal emission from the jets. The differences between subsamples may be due to the differences between accretion modes (Blandford 1984). If a radiation torus around a black hole is radiating at just over the Eddington limit, the emission is dominated by the thermal radiation, since there are insufficient relativistic electrons to power a synchrotron continuum. The radio loud quasars accrete at higher rate so that they produce the jets populated by relativistic electrons, but the synchrotron emission (and possibly SSC) need not dominate and hence we see both the thermal disk and non-thermal jet radiations. The BL Lac objects may be an extreme case with intrinsically luminouse jets and a faint optically thin accretion disk, or they may possess ordinary jets that happen to be pointed to us so that the synchrotron emission is extremely enhanced and dominates the total luminosity.

There are a few complications in any of these interpretations. One concern is possible evolution effects. If the continuum emission in various bands are intrinsically related, then correlations should appear even if the subsamples are divided into narrow redshift bins within which no evolution could occur. We find most of the $\ell_r/\ell_o/\ell_x$ correlations are present in

specified bins, but appear weaker than the correlations seen in the entire subsamples. For example, the correlation probabilities between the radio and the X-ray luminosities of the radio selected quasars are 5% for $0.0 \leq z < 0.5$, 0.01% for $0.5 \leq z < 1.0$, 0.03% for $1.0 \leq z < 1.5$, 93% for $1.5 \leq z < 2.0$, 17% for $2.0 \leq z < 2.5$, and 0.6% for $2.5 \leq z$. The low correlation probabilities in these subsamples are partly due to the reduced size of the data sets in each bin, and partly by the narrow range of luminosities in each redshift bin. The existence of the correlations within narrow redshift ranges gives some confidence, however, that the correlations are not entierly due to cosmological luminosity evolution.

Another problem is inappropriately defined samples. We subdivided our samples by selection criteria such "X-ray selected" or "optically selected" objects. This method may introduce some mixing of intrinsically different samples. For example, the optically selected quasars clearly contain a few "radio loud" quasars. Although this mixing might lead to some misleading statistical results, comparison between the "radio selected" (which are chosen from their initial discovery in radio surveys) and the "radio loud" subsamples (which are chosen from the entire sample with the condition $\alpha_{ro} > 0.3$) shows that there is no significant difference.

We thus find that, although a large number of data were collected, it proves difficult to specify a physical model. This is partly because most theoretical studies do not show tracks in α_{ox}/α_{ro} or ℓ_r / ℓ_o / ℓ_x plots. Since these kinds of plots are now widely produced observationally, we encourage theorists to make such predictions. It is also desirable to have deeper surveys in all bands so that we can examine samples with wide luminosity ranges within specific redshift ranges. These surveys may clarify the evolution effect on the emission mechanisms.

VI. SUMMARY

Using a large database, we investigated statistical properties of AGNs continuum levels in the radio, optical, and X-ray bands. For the radio luminosity of AGNs, we used the core luminosity to discount effects from radio lobes and jets. The statistical methods called survival analysis were used to show the statistical relations despite the upper limits in flux limited data sets. Our main results are as follows:

1. For the optically selected quasars and the X-ray selected AGNs, ℓ_o is correlated with ℓ_x, but not with ℓ_r. Also ℓ_r does not correlate with ℓ_x. This suggests that the main emission mechanism of these subsamples is thermal emission. For the BL Lac objects, ℓ_r/ℓ_x relation is most significant, and this suggests that the main emission mechanism of the BL Lac objects is non-thermal. The radio selected quasars show high significance levels for both ℓ_r/ℓ_x and ℓ_o/ℓ_x relations. Hence they may have both the mechanisms, which is further supported by model fitting suggesting that the radio selected quasars have two different X-ray emission mechanisms.

2. The BL Lac objects have similar emission mechanisms as the radio selected quasars, at least in the limited redshift range overlapping both samples. The radio selected BL Lac objects are perhaps special cases of the unresolved radio selected quasars. The difference between the radio selected and the X-ray selected BL Lac objects may be due either to beaming effects or selection effects.

3. Some compact radio sources with faint optical counterparts show that $\langle\alpha_{ro}\rangle \geq \langle\alpha_{ox}\rangle$. This suggests the possibility that SSC emission may be present in the optical to X-ray bands.

4. The spectral index between the optical and X-ray luminosities depends on

the optical luminosity. The optical luminosity increases faster than the X-ray luminosity.

Acknowledgements

We would like to thank D. J. Helfand and H. Kühr for providing unpublished data. One of us (K. P. S.) would like to thank Prof. G. P. Garmire for the hospitality at the Pennsylvania State University while working on this study. This work was supported in part by NASA grant NAG 8-555 and by a NSF Presidential Young Investigator Award (AST 83-51447).

Table Captions

Notes to Table 2a:

1. First detected by Condon and Dressel (1978). We find a faint radio lobe (3 mJy) 6" at P.A. 104 ° from the quasar.
2. A 6xRMS detection within 1" of the optical position.
3. A 5.5xRMS detection within 1" of the optical position. Mrk 205 was also detected by Sulentic (1986) at a level of 1.48 ± 0.25 mJy at 5 GHz.
4. First detected by Sramek and Weedman (1980). Our improved position is 12h58m59.4s, 34°16'38".
5. A 7xRMS detection within 1" of the optical position.
6. First detected by Sramek and Weedman (1980). Our improved position is 16h04m53.4s, 29°03'21".

Definitions for Table 3:

Optical

If a radio AGN has an optical "empty field", V>20.0 is used as the optical upper limit.

X-ray

If only the X-ray flux (or flux density or count number) is available, the luminosity is computed according to the descriptions below for the given reference:

* Ll X-ray list gives X-ray data in the flux density at 1 keV. The conversion to the flux (0.5-4.5 keV) is

$$S_x(0.5\text{–}4.5)[10^{-13}\ erg/sec/cm^2]=0.068\ f_x(1\text{keV})\ \text{nJy}$$

* O1 X-ray list gives the X-ray data in the flux (0.15-3.5 keV). The conversion is

$$S_x(0.5\text{–}4.5)=0.95\ S_x(0.15\text{–}3.5)$$

* B3 X-ray list gives the X-ray (0.5-3.0 keV flux). The conversion is

$$S_x(0.5\text{–}4.5)=1.38\ S_x(0.5\text{–}3.0).$$

* G2 X-ray list gives the X-ray (0.3-3.5 keV flux). The conversion is

$$S_x(0.5\text{–}4.5)=1.07\ S_x(0.3\text{–}3.5).$$

* W2 X-ray list gives the X-ray K_2 count rate. The conversion is

$$S_x=2.88\text{x}10^{-13}K_2\ erg/sec/cm^2.$$

* The X-ray flux is computed from *Einstein* IPC photon counts (cts/sec) by

$$1.0IPC(cts/sec)=3.0\text{x}10^{-11}\ erg/sec/cm^2$$

assuming $N(H)=3\text{x}10^{20}\ cm^{-2}$ and $S=(freq)^{-0.5}$.

* The X-ray flux density at 2KeV is computed by

$$S_x(2KeV)=1.47\text{x}10^{-18}f_x\ \frac{erg/sec/cm^2}{E1^{0.5}-E2^{0.5}}$$

where E1 and E2 are the band limits in KeV and f_x is in $erg/sec/cm^2$.

Notes to Table 8:

1. Data have too many upper limits and the result is obtained from a limited range.

Table 1 : Spectral Indices from Recent Literatures

Study	Spectral Indices	Descriptions
Tananbaum *et al.* (1979)	α_{ox}=1.27±0.07	Mixed QSOs
Ku *et al.* (1980)	α_{ox}=1.46±0.02	Total sample
	α_{ox}=1.38±0.03	Radio selected QSOs
	α_{ox}=1.52±0.03	Optically selected QSOs
	α_{ox}=1.41±0.03	X-ray selected AGNs
	α_{ox}=1.36±0.04	Radio QSOs with low redshift (z<1.0)
	α_{ox}=1.40±0.03	Radio QSOs with high redshift(z>1.0)
	α_{ox}=1.36±0.04	Opt. QSOs with low redshift (z<1.0)
	α_{ox}=1.65±0.04	Opt. QSOs with high redshift (z>1.0)
	α_{ox}=1.25±0.05	OVV
	α_{ox}=1.31±0.05	BL Lacs
Zamorani *et al.* (1981)	α_{ox}=1.27±0.03	Radio loud
	α_{ox}=1.46+0.05/-0.07	Radio quiet
	α_{ox}=1.35+0.05/-0.08	Radio quiet with low redshift (z<1.0)
	α_{ox}=1.62+0.08/-0.16	Radio quiet with high redshift (z>1.0)
	α_{ox}=1.37+0.05/-0.08	Radio quiet with $\log(\ell_o)$<31.4
	α_{ox}=1.62+0.08/-0.11	Radio quiet with $\log(\ell_o)$>31.4
Owen *et al.* (1981)	α_{mx}=1.02±0.05	mm selected AGNs
	α_{ox}=1.21±0.19	mm selected AGNs
Stocke *et al.*(1983)	α_{ox}=1.3±0.2	X-ray selected AGNs
Marshall *et al.* (1983)	α_{ox}=1.37±0.10	Optically selected quasars

Cruz-Gonzales and	α_{ri}=0.59±0.10	BL Lac : radio -infrared
Huchra (1984)	α_{rx}=0.94±0.09	BL Lac : radio - X-ray
Margon and Chanan	α_{ox}=1.26±0.03	X-ray selected quasars
(1985)		
Ledden and O'Dell	α_{ro}=0.63±0.12	BL Lacs
(1985)	α_{rx}=0.89±0.06	BL Lacs
	α_{ox}=1.40±0.17	BL Lacs
	α_{ro}=0.74±0.10	HPQs
	α_{rx}=0.92±0.06	HPQs
	α_{ox}=1.30±0.13	HPQs
	α_{ro}=0.67±0.12	Blazars
	α_{ox}=1.36±0.17	Blazars

Table 2a : VLA Observations of Optically Selected Quasars

Object	Name	S_6(mJy)	Note	Object	Name	S_6(mJy)	Note
0137-010	NAB	<0.8		1045+128e	nrNGC3384	<1.1	
0143-015	MC5 366	<0.8		1045+128f	nrNGC3384	<0.9	
0143-010	MC5 368	<0.8		1045+128g	nrNGC3384	<0.9	
0146+017	MC5 141	<1.2		1045+128h	nrNGC3384	<1.0	
0207-378		<1.3		1202+281	GQ Com	1.1	2
0241+011a	nrNGC1073	<2.0		1219+755	Mrk 205	0.9	3
0241+011b	nrNGC1073	<2.0		1246-057		<0.9	
0241+011c	nrNGC1073	40.5	1	1258+286	W 61972	<0.9	
0242-410		<1.4		1258+342	KP 33	25.1	4
0849+154	LB 8796	<0.9		1300-243		1.3	5
0854+194	LB 8948	1.8		1334+286	RS 23	<0.8	
0855+188	LB 8991	<0.9		1346-036		<1.0	
0856+186	LB 9010	<1.0		1604+290	KP 63	4.0	6
0856+189	LB 9029	<0.8		1606+288	KP 64	<0.9	
1045+128a	nrNGC3384	<1.0		1606+289	KP 67	<0.9	
1045+128b	nrNGC3384	<0.9		1720+246	V396 Her	31.0	
1045+128c	nrNGC3384	<0.9		1803+676		<0.8	
1045+128d	nrNGC3384	<1.0		2225-055	PHL 5200	<0.8	

Table 2b : VLA Observations of X-ray Selected AGNs.

Object	Name	S_6(mJy)	Object	Name	S_6(mJy)
0057+311	1E	<0.7	1205+465	1E	<0.7
0112+325	1E	<0.8	1228+164	1E	<0.8
0225+312	1E	<0.6	1304+341	1E	<0.7
0244+192	1E	<0.6	1352+1820	1E	<0.7
0357+104	1E	<0.7	1352+1828	1E	<1.0
0745+554	1E	<0.7	1357-022	1E	<0.7
0754+392	1E	3.6	1401+095	1E	18.8
0906+425	1E	<0.8	1529+050	1E	3.8
1008+345	1E	<0.8	1530+151	1E	<0.9
1011+032	1E	<0.7	1602+241	1E	<1.2
1031+582	1E	<0.6	1747+683	1E	<0.6
1139+104	1E	<1.1	2251-175	1E	<0.7

Table 3 : Quasar Continuum Spectra

(a) Radio Selected Quasars

Object	Name	z	ℓ_{rc}	ℓ_o	ℓ_x	α_r	α_{ro}	α_{ox}	References r	o	x
0008+171	4C17.04	1.601	35.10	31.70	45.96	...	0.63	1.43	L1	H3	L1
0017+154	3CR 9	2.012	<34.52	31.91	45.94	...	<0.49	1.52	M2	H3	Z1
0051+291	4C 29.01	1.828	<34.65	31.99	46.75	...	<0.49	1.24	V2	H3	J2
0056-001	4C-00.06	0.720	<34.55	31.01	44.92	0.45	<0.66	1.57	L1	H3	L1
0106+013	4C 01.02	2.107	36.07	31.88	46.58	-0.49	0.78	1.28	P2	H3	O1
0109+176	4C 17.09	2.157	33.64	32.08	<46.19	...	0.29	>1.49	F1	H3	K1
0112-017	PKS	1.365	35.04	31.71	46.11	-0.45	0.62	1.37	P2	H3	Z1
0119+041	PKS	0.637	34.19	30.01	45.20	0.01	0.78	1.07	P2	H3	O1
0119-046	4C-04.04	1.948	<35.23	31.18	46.73	...	<0.75	0.93	V2	H3	J2
0133+207	3CR 47	0.425	32.68	30.17	45.72	...	0.47	0.93	M2	H3	Z1
0134+329	3CR 48	0.367	<34.54	30.84	45.43	0.85	<0.69	1.30	R2	H3	T1
0135-247	PKS	0.831	34.64	31.29	45.68	-0.17	0.62	1.38	L1	H3	L1
0205+024	NAB	0.155	30.32	30.25	44.47	...	0.01	1.44	V2	H3	W2
0229+131	4C 13.14	2.065	35.73	32.14	46.49	-0.46	0.67	1.39	K2	H3	O1
0229+341	3CR 68.1	1.228	<34.79	31.03	45.28	0.45	<0.70	1.43	B3	H3	B3
0234+285	4C 28.07	1.213	35.24	31.18	46.04	0.00	0.75	1.20	K2	H3	O1
0237+040	OD 062	0.978	34.49	30.83	45.51	-0.10	0.68	1.27	P2	H3	H1
0237-027	PKS	1.116	34.84	30.64	45.70	...	0.78	1.12	P2	O1	O3
0237-233	PKS	2.223	<35.95	32.65	47.16	0.48	<0.62	1.33	P2	H3	K1
0312-770	PKS	0.223	33.08	30.42	44.99	0.05	0.49	1.31	V2	H3	Z1
0313+344	4C 34.13	1.156	<33.57	31.25	45.43	<0.85	<0.43	1.46	C5	H3	C6
0333+321	4C 32.14	1.258	35.32	31.78	46.68	0.15	0.66	1.18	P2	H3	M4
0336-019	CTA 26	0.852	34.99	30.74	45.43	-0.19	0.79	1.26	K2	H3	H1
0400+258	B2	2.109	35.48	32.16	<45.76	-0.21	0.62	>1.68	P2	H3	H1
0403-132	PKS	0.571	<34.69	30.85	45.40	0.31	<0.71	1.32	K2	H3	B2
0409+229	3C 108	1.215	34.70	31.18	45.54	-0.14	0.65	1.39	B3	H3	B3
0414-060	3C 110	0.781	<33.96	32.07	45.89	...	<0.35	1.60	V2	H3	Z1
0420-014	PKS	0.915	35.17	31.11	46.12	-1.00	0.76	1.14	P2	H3	K1
0424-131	PKS	2.165	<34.85	32.31	45.96	0.80	<0.47	1.66	F1	H3	Z1
0438-436	PKS	2.852	<36.21	32.14	46.95	0.36	<0.76	1.22	P2	H3	Z1
0440-003	NRAO 190	0.850	34.60	30.46	45.82	0.40	0.77	1.01	P2	H3	K1
0454-234	PKS	1.009	34.99	31.15	45.74	0.09	0.71	1.30	P2	P2	H1
0458-020	4C-02.19	2.286	35.74	32.04	46.19	-0.19	0.63	1.47	K2	H3	H1
0518+165	3CR 138	0.760	<35.05	30.80	45.40	0.67	<0.79	1.30	P2	H3	Z1
0528-250	PKS	2.765	35.66	32.58	46.98	0.28	0.57	1.37	P2	H3	Z1
0537-441	PKS	0.894	35.18	32.00	45.79	0.10	0.59	1.61	P2	H3	Z1
0537-286	PKS	3.110	35.89	31.82	47.20	-0.34	0.76	1.00	P2	H3	Z1
0538+498	3CR 147	0.545	<35.02	30.86	44.93	0.85	<0.77	1.50	P2	H3	Z1
0607-157	PKS	0.324	<33.48	30.11	44.53	0.76	<0.63	1.37	K2	H3	H1
0637-752	PKS	0.651	35.09	31.62	46.36	-0.08	0.65	1.24	K2	H3	Z1
0642+449	OH 471	3.400	35.77	32.69	47.20	0.14	0.57	1.33	P2	H3	Z1
0710+118	3CR 175	0.768	<32.58	31.57	45.34	...	<0.19	1.62	M2	H3	Z1
0723-008	PKS	0.128	33.15	29.36	44.09	0.16	0.70	1.25	P2	O1	O3
0736+017	PKS	0.191	33.55	30.35	44.44	0.01	0.59	1.49	O2	H3	K1
0738+313	B2	0.630	34.46	31.08	45.32	0.17	0.63	1.44	P2	H3	H1
0740+380	3CR 186	1.063	<34.37	31.39	45.77	1.02	<0.55	1.38	R1	H3	Z1
0758+140	3CR 190	1.197	<34.80	30.80	45.38	0.91	<0.78	1.23	B3	B3	B3
0802+103	3CR 191	1.956	<35.10	31.90	46.15	0.67	<0.59	1.43	J1	H3	T1
0805+046	4C 05.34	2.877	35.16	32.52	46.55	...	0.49	1.52	F1	H3	K1
0809+483	3CR 196	0.871	<34.15	31.02	45.28	...	<0.58	1.43	P1	H3	Z1

Object	Name	z	ℓ_{rc}	ℓ_o	ℓ_x	α_r	α_{ro}	α_{ox}	References r	o	x
0824+110	MC5	2.278	34.87	31.80	46.34	0.19	0.57	1.32	V2	H3	J2
0827+243	OJ 248	0.939	34.39	31.24	45.53	0.04	0.59	1.42	O3	H3	O1
0830+112	MC5	0.589	<31.19	30.79	44.90	...	<0.07	1.49	F1	H3	K1
0830+115	MC5	2.974	<35.15	32.36	<46.91	0.35	<0.52	>1.32	F1	H3	K1
0833+654	3CR 204	1.112	33.42	31.16	45.87	...	0.42	1.26	M2	H3	Z1
0834-20	PKS	2.752	<36.22	32.16	46.87	...	<0.75	1.26	V2	V2	H1
0835+580	3CR 205	1.534	33.57	31.82	45.99	...	0.33	1.46	P1	H3	Z1
0837-120	3CR 206	0.200	32.44	29.72	45.16	0.02	0.43	0.98	M2	H3	W2
0838+133	3CR 207	0.684	34.04	30.69	45.46	...	0.62	1.23	P1	H3	Z1
0850+140	3CR 208	1.110	33.38	31.49	45.77	...	0.35	1.42	M2	H3	Z1
0855+143	3CR 212	1.049	<34.67	30.53	45.16	0.84	<0.77	1.14	B2	H3	B2
0903+169	3CR 215	0.411	<32.05	30.07	45.15	...	<0.37	1.11	P1	H3	Z1
0906+015	4C 01.24	1.018	34.88	31.32	45.85	-0.53	0.66	1.32	K2	H3	K1
0906+431	3CR 216	0.668	<34.56	30.49	45.16	0.56	<0.76	1.27	B3	H3	B3
0923+392	4C 39.25	0.699	35.23	30.79	45.92	-1.15	0.83	1.09	P2	H3	Z1
0938+119	MC5	3.183	<35.05	32.23	<46.43	0.42	<0.52	>1.45	F1	H3	Z1
0953+254	OK 290	0.712	34.53	30.96	45.70	-0.60	0.38	1.24	P2	H3	O1
0959-443	PKS	0.84	34.44	32.01	45.58	...	0.45	1.70	V2	V2	W2
1004+130	4C13.41	0.240	31.60	30.77	<44.15	0.18	0.15	>1.77	F1	H3	Z1
1004-217	PKS	0.330	33.16	30.66	44.38	...	0.47	1.56	V2	H3	Z1
1023+067	3CR 243	1.699	<34.15	32.29	<46.04	...	<0.35	>1.62	M2	H3	Z1
1028+313	B2	0.177	32.09	29.85	44.94	...	0.42	1.11	F1	H3	Z1
1038+064	4C 06.41	1.270	<35.02	31.86	46.56	...	<0.59	1.26	V2	H3	J2
1040+123	3CR 245	1.029	34.76	31.39	45.86	0.60	0.63	1.35	J1	H3	T1
1058+726	W1	0.375	<33.51	30.13	44.61	0.62	<0.63	1.34	F1	H3	K1
1100+772	3CR249.1	0.311	<32.50	30.81	45.23	...	<0.31	1.37	M2	H3	Z1
1111+408	3C 254	0.734	34.02	30.77	45.69	1.20	0.61	1.17	M2	H3	T1
1127-145	PKS	1.187	35.50	31.75	46.10	0.25	0.70	0.90	P2	H3	H1
1137+660	3CR 263	0.652	33.49	31.32	45.98	...	0.40	1.27	M2	H3	Z1
1157+014	PKS	1.986	<34.41	32.35	44.97	...	<0.38	2.06	V2	H3	B2
1207-399	PKS	0.966	34.28	31.55	45.63	0.02	0.51	1.50	F1	H3	Z1
1217+023	PKS	0.240	32.95	30.20	45.41	-0.43	0.51	1.06	F1	H3	Z1
1219+04	PKS	0.967	34.62	31.28	46.24	...	0.62	1.16	V2	V2	O1
1223+252	4C 25.40	0.268	31.09	30.52	44.52	0.64	0.11	1.53	F1	H3	Z1
1225+317	B2	2.230	34.95	32.95	46.68	-0.06	0.37	1.63	F1	H3	Z1
1226+023	3CR 273	0.158	34.51	31.28	46.23	0.04	0.60	1.16	P2	H3	K1
1229-021	4C-02.55	1.038	<34.76	31.60	45.74	0.48	<0.59	1.48	K2	H3	J2
1237-101	PKS	0.753	34.39	31.00	45.32	0.26	0.63	1.40	P2	H3	Z1
1250+568	3CR277.1	0.321	<33.67	29.93	44.35	0.64	<0.70	1.37	K2	H3	K1
1252+119	PKS	0.871	34.48	31.44	45.76	0.15	0.57	1.40	P2	H3	Z1
1253-055	3C 279	0.538	35.09	30.53	46.04	-0.28	0.85	0.95	P2	H3	Z1
1258+286	5C 04.12	1.373	<34.22	31.08	45.71	...	<0.58	1.29	F1	H3	K1
1258+287	5C04.105	0.650	33.15	31.62	45.06	0.00	0.28	1.74	F1	H3	K1
1328+254	3CR 287	1.055	<35.25	31.26	45.72	0.61	<0.74	1.35	P2	H3	T1
1328+307	3CR 286	0.849	<35.40	31.16	45.40	0.55	<0.79	1.44	P2	H3	T1
1331+170	MC3	2.081	35.18	32.81	46.34	-0.40	0.44	1.71	F1	H3	Z1
1340+606	3CR288.1	0.961	<34.07	30.97	45.11	...	<0.58	1.47	P1	H3	Z1
1402+044	PKS	3.200	35.64	32.40	46.26	0.02	0.60	1.58	F1	H3	Z1
1402-012	PKS	2.518	35.38	32.12	46.20	0.10	0.60	1.50	P2	H3	Z1
1413+135	PKS	0.26	33.54	28.81	44.02	-0.07	0.88	1.06	B3	B3	B3

Table 3(a) - Continued

Object	Name	z	ℓ_{rc}	ℓ_o	ℓ_x	α_r	α_{ro}	α_{ox}	References r	o	x
1416+067	3CR 298	1.439	<35.19	32.03	46.04	0.52	<0.59	1.52	K2	H3	Z1
1422+202	4C 20.33	0.871	33.07	30.99	45.51	...	0.39	1.31	F1	H3	H1
1425+267	B2	0.366	32.55	30.96	44.52	0.11	0.30	1.70	M2	H3	W2
1435+248	4C 24.32	1.010	<34.01	30.67	45.45	0.54	<0.62	1.23	V2	H3	K1
1442+101	OQ 172	3.530	<36.04	32.83	47.06	0.60	<0.60	1.44	P2	H3	K1
1458+718	3CR309.1	0.905	<35.25	31.45	45.87	0.68	<0.71	1.37	R2	H3	Z1
1502+106	PKS	1.833	35.61	32.86	<45.89	0.03	0.51	>1.90	H1	H3	H1
1504-167	MC	0.876	35.01	30.75	45.75	-0.28	0.79	1.14	P2	H3	H1
1510-089	PKS	0.361	34.27	30.64	45.30	-0.29	0.67	1.27	P2	H3	K1
1512+370	4C37.43	0.371	32.69	31.05	45.21	0.18	0.30	1.47	M2	H3	W2
1522+155	MC 3	0.628	<33.72	30.81	45.34	...	<0.54	1.33	L2	H3	L2
1524+101	4C 10.43	1.358	34.04	31.48	45.69	...	0.48	1.45	F1	H3	Z1
1525+227	B2	0.253	<32.59	30.32	43.64	...	<0.42	1.79	V2	H3	W2
1545+210	3CR323.1	0.264	31.96	30.25	45.30	...	0.32	1.12	M2	H3	K1
1546+027	PKS	0.413	33.24	30.17	45.41	-0.70	0.57	1.05	P2	H3	Z1
1548+114	4C 11.50	0.436	33.51	30.63	45.46	-0.63	0.54	1.21	F1	H3	Z1
1555+001	DA 393	1.770	35.20	31.33	<45.78	0.02	0.72	>1.36	P2	H3	H1
1555+332	GC	0.942	33.48	30.88	45.15	0.32	0.48	1.42	F1	H3	Z1
1556+335	GC	1.650	<34.20	32.13	45.82	0.36	<0.38	1.65	F1	H3	Z1
1606+289	4C 28.40	1.989	<34.70	31.58	45.70	1.12	<0.58	1.48	R1	H3	K1
1611+343	DA 406	1.404	35.36	31.73	45.84	0.01	0.67	1.49	K2	H3	H1
1618+177	3CR 334	0.555	33.31	31.13	45.32	0.20	0.41	1.45	M2	H3	T1
1622+238	3CR 336	0.927	33.07	31.20	45.41	...	0.35	1.45	F1	H3	T1
1623+269	4C 26.48	0.779	<32.95	31.06	45.16	...	<0.35	1.49	F1	H3	K1
1632+391	4C 39.46	1.082	<34.35	31.18	<45.61	0.62	<0.59	>1.36	I1	H3	K1
1633+382	4C 38.41	1.814	35.60	31.87	46.23	-0.15	0.69	1.39	P2	H3	K1
1635+119	MC2	0.146	31.22	29.59	44.43	-0.25	0.30	1.21	F1	H3	Z1
1641+399	3C 345	0.595	35.09	31.38	45.96	-0.09	0.69	1.31	P2	H3	K1
1704+608	3CR 351	0.371	32.03	31.18	44.97	...	0.16	1.61	M2	H3	Z1
1725+044	PKS	0.293	33.53	29.86	44.12	-0.29	0.68	1.43	P2	H3	K1
1729+501	4C 50.43	1.111	33.36	31.46	<45.77	0.27	0.35	>1.41	F1	H3	K1
1730-13	NRAO530	0.902	35.21	31.06	45.81	...	0.77	1.24	V2	V2	H1
1739+522	4C 51.37	1.375	34.94	31.35	46.15	-0.04	0.67	1.22	P2	H3	H1
1756+237	PKS	1.721	35.02	31.90	46.08	...	0.58	1.46	V2	H3	J2
1828+487	3C 380.0	0.692	<34.52	31.26	45.94	0.56	<0.61	1.27	U1	H3	Z1
1928+738	4C73.18	0.36	34.30	31.10	45.39	0.03	0.59	1.42	B1	B1	B1
2037+511	3CR 418	1.686	35.75	31.69	46.12	0.27	0.75	1.36	P2	H3	K1
2120+168	3CR 432	1.805	33.10	31.94	45.71	...	0.22	1.62	F1	H3	Z1
2121+053	OX 036	1.878	<35.31	32.13	46.45	0.30	<0.59	1.40	F1	H3	K1
2126-158	PKS	3.270	35.90	32.93	47.76	-0.48	0.55	1.21	P2	H3	Z1
2128-123	PKS	0.501	34.53	31.18	45.46	-0.69	0.62	1.12	K2	H3	W2
2135-147	PKS	0.200	32.22	30.45	45.23	...	0.33	1.23	M2	H3	Z1
2141+175	PKS	0.213	<32.82	30.60	44.20	0.32	<0.41	1.68	F1	H3	Z1
2143-156	PKS	0.700	34.27	30.93	45.53	0.20	0.65	1.30	L1	H3	L1
2145+067	PKS	0.990	35.07	31.70	46.36	0.13	0.63	1.27	P2	H3	J2
2201+315	4C 31.63	0.297	33.71	30.97	45.42	0.08	0.51	1.36	P2	H3	H1
2216-038	4C-03.79	0.901	35.15	31.60	45.80	-1.38	0.66	1.45	P2	H3	K1
2223+210	DA 580	1.960	<35.44	32.00	47.04	0.61	<0.64	1.13	K2	H3	J2
2223-052	3C 446	1.404	35.73	31.37	46.98	0.27	0.81	0.91	K2	H3	Z1
2230+114	4C 11.69	1.037	<35.32	31.40	46.32	0.35	<0.73	1.17	P2	H3	Z1
2234+282	B2	0.795	34.79	30.54	45.13	-0.25	0.79	1.30	L2	H3	L2
2251+113	4C 11.72	0.323	31.98	30.81	<44.91	...	0.22	>1.49	F1	H3	K1
2251+158	3CR454.3	0.859	35.55	31.67	46.30	-0.04	0.72	1.29	P2	H3	T1
2254+024	PKS	2.090	35.00	32.03	45.99	-0.30	0.55	1.54	F1	H3	Z1
2344+092	4C 09.74	0.677	34.55	31.48	45.77	0.00	0.57	1.42	P2	H3	Z1
2345-167	PKS	0.600	<34.46	30.54	45.24	0.32	<0.77	1.26	P2	H3	K1

(b) Optically Selected Quasars

Object	Name	z	ℓ_{rc}	ℓ_o	ℓ_x	α_{ro}	α_{ox}	References r	o	x
0026+129	PG	0.142	30.20	30.42	44.90	-0.04	1.34	C2	H3	Z1
0051+146	PHL 891	0.874	<32.34*	30.83	<45.18	<0.28	>1.39	S3	H3	Z1
0052+145	PHL 892	0.911	<32.40*	30.83	<45.00	<0.29	>1.46	S3	H3	Z1
0054+144	PHL 909	0.171	<30.10	29.83	44.75	<0.05	1.17	C2	H3	Z1
0100+130	PHL 957	2.690	<32.67	32.94	<46.54	<-0.05	>1.68	C2	H3	K1
0130+033	PHL 1027	0.363	<31.75*	30.41	44.91	<0.25	1.34	S3	H3	Z1
0131+037	PHL 1033	0.255	<31.38*	29.40	44.67	<0.37	1.04	S3	H3	Z1
0134+033	PHL 1070	0.079	<30.43+	28.75	42.71	<0.31	1.54	S3	H3	Z1
0137+060	PHL 1092	0.396	<31.98*	30.52	44.30	<0.27	1.61	S3	H3	Z1
0137-010	NAB	0.334	<30.59	30.53	44.88	<0.01	1.39	I1	H3	Z1
0143-015	MCS 366	3.190	<32.27	32.27	<46.61	<0.09	>1.40	I1	H3	Z1
0143-010	MCS 368	3.240	<32.77	32.21	<46.38	<0.10	>1.46	I1	H3	Z1
0145+042	UM 139	2.030	<32.61	31.67	<45.92	<-0.17	>1.44	S3	H3	B4
0146+017	MCS 141	2.920	<32.83	32.23	<46.28	<0.11	>1.51	I1	H3	Z1
0205-379		2.420	34.00	32.53	46.28	0.27	1.63	C3	H3	Z1
0207-398		2.805	<32.83	32.61	46.43	<0.04	1.60	I1	H3	Z1
0241+011	nr N1073	1.945	<32.63	31.30	<45.75	<0.25	>1.36	I1	A1	K1
0241+011	nr N1073	0.599	<31.51	30.19	<44.41	<0.25	>1.44	I1	A1	K1
0241+011	nr N1073	1.411	33.62	30.69	<45.35	0.54	>1.27	I1	A1	K1
0242-410		2.214	<32.61	32.06	<45.86	<0.10	>1.60	I1	H3	Z1

Table 3(b) - Continued

Object	Name	z	ℓ_{rc}	ℓ_o	ℓ_x	α_{ro}	α_{ox}	References r	o	x
0420-388		3.120	34.85	33.02	46.85	0.34	1.59	C3	H3	Z1
0805+044	KP 2	2.060	<33.69*	31.42	<46.23	<0.42	>1.22	S3	S3	K1
0847+153	KP 3	2.190	<33.16*	31.28	<46.31	<0.35	>1.13	S3	S3	K1
0847+153	KP 4	2.660	<32.66	31.94	<46.54	<0.13	>1.30	S3	S3	K1
0847+153	KP 5	2.200	<32.46	30.88	<46.32	<0.29	>0.98	S3	S3	K1
0848+155	LB 8755	2.010	34.57	32.15	46.02	0.45	1.58	S3	H3	K1
0849+154	LB 8796	1.320	<31.91	31.50	<45.67	<0.07	>1.46	I1	H3	K1
0854+194	LB 8948	0.331	30.94	30.22	<44.23	0.16	>1.52	I1	H3	K1
0855+188	LB 8991	1.013	<31.65	31.45	<45.36	<0.04	>1.56	I1	H3	K1
0856+186	LB 9010	1.711	<32.21	31.69	<45.98	<0.09	>1.42	I1	H3	K1
0856+189	LB 9089	1.286	<31.83	31.57	<45.63	<0.05	>1.50	I1	H3	K1
1011+250	Ton 490	1.633	34.96	32.75	46.60	0.41	1.59	C2	H3	K1
1045+128	nr N3384	1.111	<31.79	30.68	<45.59	<0.20	>1.18	I1	H3	K1
1045+128	nr N3384	1.107	<31.74	30.44	<45.59	<0.24	>1.09	I1	H3	K1
1045+128	nr N3384	1.131	<31.76	30.55	<45.61	<0.22	>1.12	I1	H3	K1
1045+128	nr N3384	1.134	<31.81	30.95	<45.62	<0.16	>1.27	I1	H3	K1
1045+128	nr N3384	1.192	<31.89	30.82	<45.67	<0.20	>1.20	I1	H3	K1
1045+128	nr N3384	1.280	<31.88	30.68	<45.75	<0.22	>1.12	I1	H3	K1
1045+128	nr N3384	0.520	<31.04	29.40	<44.80	<0.30	>0.99	I1	H3	K1
1045+128	nr N3384	0.497	<31.05	29.31	<44.75	<0.32	>0.98	I1	H3	K1
1202+281	GQ Com	0.165	30.11	30.25	45.04	-0.03	1.22	I1	H3	Z1
1219+755	Mkn 205	0.070	29.28	29.90	44.46	-0.12	1.31	I1	H3	Z1
1229+204	Ton 1542	0.064	<29.98*	29.47	43.90	<0.09	1.36	S3	H3	W2
1243+346	KP 22	2.290	<34.00*	31.43	<46.08	<0.48	>1.28	S3	S3	Z1
1244+345	KP 23	1.940	<33.41*	31.21	<45.87	<0.41	>1.27	S3	S3	Z1
1244+346	KP 24	2.200	<33.83*	30.81	<46.20	<0.56	>0.99	S3	S3	Z1
1244+346	KP 25	2.240	<32.52*	31.12	<46.28	<0.26	>1.14	S3	S3	Z1
1244+347	KP 26	2.490	<32.70	31.90	<46.18	<0.15	>1.42	S3	S3	Z1
1245+345	B 19	2.070	<33.65*	31.98	<46.18	<0.31	>1.45	S3	H3	Z1
1245+343	KP 27	1.700	<33.63*	30.76	<45.94	<0.53	>1.07	S3	S3	Z1
1245+342	KP 28	1.700	<33.54*	30.88	<45.65	<0.49	>1.23	S3	S3	Z1
1246+344	KP 29	2.230	<32.67	31.51	<46.04	<0.22	>1.32	S3	S3	Z1
1246-057		2.212	<32.42	32.50	<45.93	<-0.02	>1.75	I1	H3	K1
1246+335	B 46	0.271	<30.51	29.80	44.32	<0.13	1.33	S3	H3	Z1
1257+346	B 201	1.375	33.11	31.97	<45.73	0.21	>1.62	C2	H3	K1
1258+286	W 61972	1.922	<32.28	32.00	<46.26	<0.05	>1.43	I1	H3	K1
1258+340	B 246	0.690	<32.60*	30.61	<44.91	<0.37	>1.41	S3	H3	K1
1258+343	B 471	0.774	<32.63*	30.95	<45.06	<0.31	>1.49	S3	H3	K1
1258+342	KP 31	2.010	<34.03*	31.45	<46.21	<0.48	>1.24	S3	S3	K1
1258+343	KP 32	1.800	<33.79*	30.87	<46.05	<0.54	>1.07	S3	S3	K1

Object	Name	z	ℓ_{rc}	ℓ_o	ℓ_x	α_{ro}	α_{ox}	References r	o	x
1258+342	KP 33	1.930	33.72	31.20	<46.11	0.47	>1.18	I1	S3	K1
1259+347	KP 34	2.080	<32.40	30.98	<46.24	<0.26	>1.04	S3	S3	K1
1259+344	KP 35	2.820	<33.97*	32.11	<46.69	<0.35	>1.31	S3	S3	K1
1259+344	BSO 6	1.956	<33.62*	31.98	<46.13	<0.30	>1.47	S3	H3	K1
1300+345	KP 36	2.880	<33.97*	31.90	<46.73	<0.39	>1.21	S3	S3	K1
1300+344	KP 37	1.700	<32.15	31.12	<45.97	<0.19	>1.20	S3	S3	K1
1300+343	KP 38	1.800	<33.51*	30.79	<46.05	<0.51	>1.04	S3	S3	K1
1300-243		2.259	32.60	32.57	<46.40	0.00	>1.39	I1	H3	Z1
1303+308	W22722	1.770	<33.10*	31.93	<46.25	<0.22	>1.40	S3	H3	K1
1303+313	W21541	2.047	<33.32*	32.10	46.44	0.23	1.40	S3	H3	K1
1309-056		2.180	<34.08	32.24	46.45	<0.30	1.54	Z1	H3	Z1
1311+362	BSO 11	2.084	<33.69*	31.85	45.93	<0.34	1.50	S3	H3	J2
1318+290	Ton 155	1.703	<33.25*	32.19	<46.15	<0.20	>1.54	S3	H3	Z1
1318+290	Ton 156	0.549	<31.13	31.08	<44.62	<0.01	>1.70	C2	H3	Z1
1333+286	RS 23	1.910	<32.22	31.60	<46.15	<0.11	>1.32	I1	H3	Z1
1346-036		2.344	<32.52	32.58	<46.32	<-0.01	>1.63	I1	H3	Z1
1351+640	PG	0.088	31.03	29.96	43.15	0.20	1.84	C2	H3	Z1
1517+235	LB 9612	1.901	<33.15*	32.55	<46.28	<0.11	>1.63	S3	H3	Z1
1544+212	KP 57	2.050	<33.04*	30.74	<46.22	<0.43	>0.96	S3	S3	K1
1545+209	KP 58	1.850	<33.26	30.61	<46.08	<0.49	>0.96	S3	S3	K1
1548+113	KP 62	1.901	<33.24	31.13	46.40	<0.39	1.04	S3	H3	Z1
1604+290	KP 63	1.950	32.93	31.52	<45.72	0.26	>1.45	I1	S3	K1
1605+288	KP 64	1.800	<32.21	30.58	<45.61	<0.30	>1.13	I1	S3	K1
1606+291	KP 65	0.060	<30.27*	27.25	<42.25	<0.56	>1.14	S3	S3	K1
1606+290	KP 66	2.000	<33.32*	31.56	<45.75	<0.33	>1.45	S3	S3	K1
1606+289	KP 67	2.560	<32.57	31.29	<46.11	<0.24	>1.21	I1	S3	K1
1607+287	KP 68	2.300	<33.34*	31.50	<45.95	<0.34	>1.36	S3	S3	K1
1607+290	KP 69	0.350	<31.46*	29.22	<43.85	<0.42	>1.29	S3	S3	K1
1612+261	Ton 256	0.131	31.32	30.11	44.53	0.22	1.37	S3	H3	K1
1612+266	NAB	0.395	<31.68*	30.41	44.40	<0.24	1.53	S3	H3	K1
1622+268	KP 70	2.100	<33.17*	30.95	<45.82	<0.41	>1.19	S3	S3	K1
1622+269	KP 71	3.20	<33.80*	31.83	<45.88	<0.37	>1.51	S3	S3	K4
1623+271	KP 72	1.44	<33.83*	31.06	45.81	<0.51	1.24	S3	S3	K4
1623+270	KP 73	2.44	<33.46	30.98	<45.41	<0.46	>1.36	S3	S3	K4
1623+269	KP 74	1.71	<32.89*	30.79	<45.04	<0.39	>1.43	S3	S3	K4
1623+268	KP 76	2.49	<33.01	31.97	<45.48	<0.19	>1.71	S3	S3	K4
1623+269	KP 77	2.54	<33.03	32.50	45.82	<0.10	1.79	S3	S3	K4
1623+268	KP 78	2.64	<33.55*	32.93	<45.56	<0.12	>2.05	S3	S3	K4
1624+269	KP 79	2.20	<32.77	31.56	45.51	<0.24	1.52	S3	S3	K4
1720+246	V396 Her	0.175	31.62	30.01	44.04	0.03	1.52	I1	H3	Z1
1803+676		0.136	<29.80	29.97	44.41	<-0.03	1.36	I1	H3	Z1
2204-408		3.180	31.34	32.80	46.51	-0.27	1.64	C3	H3	Z1
2225-055	PHL 5200	1.981	<32.26	32.08	<46.52	<0.03	>1.36	I1	H3	Z1

(c) X-ray Selected Active Galactic Nuclei

Object	Name	z	ℓ_{rc}	ℓ_o	ℓ_x	α_{ro}	α_{ox}	References r	o	x
0007-14	E	0.456	<30.66	29.61	44.9	<0.20	1.03	H4	M3	M3
0031-077	E	0.388	<31.42	29.89	44.5	<0.28	1.29	H4	M3	M3
0031-076	E	0.291	<30.56	29.84	44.6	<0.13	1.24	H4	M3	M3
0032-073	E	0.752	<31.11	30.78	45.3	<0.06	1.33	H4	M3	M3
0037+061	E	0.063	<29.23	28.78	43.3	<0.08	1.33	H4	M3	M3
0037-019	E	0.296	<30.81	29.92	44.02	<0.17	1.49	G1	G2	G2
0038+324	E	0.197	<30.26	29.43	43.57	<0.15	1.47	G1	G2	G2
0038+328	E	0.225	<30.72	29.49	43.94	<0.24	1.32	G1	G2	G2
0038-015	E4C-02.04	1.690	34.00	32.20	45.98	0.33	1.61	G1	G2	G2
0044-209	E,PHL6625	0.380	<30.80	29.76	44.5	<0.19	1.24	H4	M3	M3
0057+311	E	0.287	<30.40	29.65	44.48	<0.14	1.21	I1	K3	K3
0100+020	E,PHL 959	0.392	<30.53	30.74	44.7	<-0.04	1.54	H4	M3	M3
0104+318	E	2.027	<32.33	31.76	46.24	<0.10	1.34	G1	G2	G2
0111-015	E	0.120	<30.12	28.49	43.44	<0.30	1.16	G1	S4	S4
0112-017	E	0.284	<31.74	29.06	43.77	<0.50	1.26	G1	S4	S4
0112+329	E	0.764	<31.34	30.51	45.28	<0.15	1.23	I1	K3	K3
0120+092	E	0.176	<29.82	29.25	43.7	<0.11	1.36	H4	M3	M3
0135+036	E	0.637	<31.17	30.33	44.79	<0.16	1.35	G1	S4	S4
0136+060	E	0.450	31.42	30.01	44.38	0.26	1.39	G1	S4	S4
0144-009	E	0.080	<29.34	29.56	43.39	<-0.04	1.59	G1	S4	S4
0149-166	E	0.399	<30.84	29.59	44.9	<0.23	1.03	H4	M3	M3
0214-033	E	0.323	<30.36	30.39	44.4	<-0.01	1.53	H4	M3	M3
0225+313	E	0.058	<28.94	28.87	43.38	<0.01	1.33	I1	K3	K3
0240+007	E,PHL1443	0.569	<31.46	31.09	44.8	<0.07	1.64	H4	M3	M3
0244+194	E	0.176	<29.91	29.89	44.26	<0.00	1.39	I1	K3	K3
0302-223	E,Ton 317	1.409	<31.70	32.16	46.1	<-0.09	1.55	H4	M3	M3
0318-196	E	0.104	<29.66	30.10	43.2	<0.08	1.87	H4	M3	M3
0331-053	E	0.139	<29.96	29.42	43.49	<0.10	1.50	G1	G2	G2
0335-350	E	0.321	<30.95	29.43	44.7	<0.28	1.04	H4	M3	M3
0336-354	E	1.002	<31.98	30.35	45.5	<0.30	1.09	H4	M3	M3
0350-280	E	0.170	<30.39	29.22	43.9	<0.22	1.27	H4	M3	M3
0351+026	E	0.036	<28.74	28.65	43.2	<0.02	1.32	H4	M3	M3
0357+107	E	0.182	<30.00	29.89	44.38	<0.02	1.34	I1	K3	K3
0412-081	E	0.037	29.05	29.00	43.16	0.01	1.47	G1	S4	S4
0420+003	E	2.903	34.27	32.09	46.8	0.41	1.26	H4	M3	M3
0438-108	E	0.868	32.98	30.06	45.37	0.54	1.02	G1	S4	S4
0440-109	E	0.279	<30.74	29.49	44.02	<0.23	1.32	G1	S4	S4
0447-092	E	0.946	<31.63	30.83	45.15	<0.15	1.40	G1	S4	S4
0449-183	E	0.338	30.74	29.80	44.68	0.17	1.19	G1	S4	S4
0450-182	E	0.059	29.59	29.45	42.94	0.03	1.72	G1	S4	S4
0457-059	E	0.303	<30.50	29.93	44.28	<0.11	1.39	G1	G2	G2
0721+690	E	0.111	<29.42	29.43	44.0	<0.00	1.31	H4	M3	M3
0745+557	E	0.174	<29.96	29.44	43.79	<0.10	1.39	I1	K3	K3
0754+374	E	0.096	30.15	30.28	44.08	-0.02	1.60	I1	K3	K3
0809+481	E	0.459	<32.30	29.87	44.45	<0.45	1.31	G1	S4	S4
0829+111	E	0.453	<31.26	29.43	44.8	<0.34	1.00	H4	M3	M3
0838+133	E	0.723	<31.63	30.17	44.78	<0.27	1.29	G1	S4	S4
0844+377	E	0.451	<30.65	30.39	44.8	<0.05	1.37	H4	M3	M3
0845+378	E	0.307	<30.31	29.92	44.2	<0.05	1.34	H4	M3	M3
0849+287	E, B2	1.273	34.44	30.55	45.31	0.72	1.24	G1	S4	S4
0849+284	E	0.209	<30.45	28.53	43.63	<0.36	1.11	G1	S4	S4
0849+284	E	0.197	<30.37	29.27	43.61	<0.20	1.40	G1	S4	S4
0850+284	E	1.273	<32.19	30.62	45.26	<0.29	1.28	G1	S4	S4
0850+284	E	0.922	33.18	31.11	44.89	0.38	1.61	G1	S4	S4
0906+254	E	0.242	<30.31	29.58	44.18	<0.14	1.30	I1	K3	K3
0906-091	E	0.129	<29.85	29.00	42.9	<0.16	1.57	H4	M3	M3
0907-091	E	0.253	<30.44	29.76	43.6	<0.13	1.59	H4	M3	M3
0911+402	E	0.323	<30.66	29.33	44.5	<0.25	1.08	H4	M3	M3
0919+515	E	0.161	<29.74	29.30	44.2	<0.08	1.18	H4	M3	M3
0937+118	E	0.783	<31.63	30.62	45.01	<0.19	1.38	G1	S4	S4
1008+348	E	0.144	<29.86	29.30	44.26	<0.10	1.16	I1	K3	K3
1011+034	E	0.313	<30.48	30.00	44.32	<0.09	1.40	I1	K3	K3
1018+201	E	0.250	<30.51	29.45	44.24	<0.20	1.22	G1	G2	G2
1031+583	E	0.248	<30.21	29.41	43.11	<0.15	1.64	I1	K3	K3
1059+730	E	0.089	<29.23	29.37	43.3	<-0.03	1.56	H4	M3	M3
1112+409	E	0.076	<29.44	28.92	43.74	<0.09	1.21	G1	G2	G2
1137+659	E	0.397	<30.99	29.53	44.20	<0.27	1.27	G1	G2	G2
1139+106	E	0.150	<30.03	28.77	44.20	<0.23	0.98	I1	K3	K3
1205+469	E	0.102	<29.50	29.00	43.64	<0.09	1.28	I1	K3	K3
1205+644	E	0.105	<29.98	28.97	43.55	<0.19	1.31	G1	G2	G2
1216+695	E	0.627	31.15	31.00	45.2	0.03	1.45	H4	M3	M3
1218+753	E	0.645	<32.28	30.58	44.95	<0.31	1.39	G1	G2	G2
1219+047	E	0.094	<29.88	29.22	43.6	<0.12	1.38	H4	M3	M3
1223+258	E	0.067	<29.24	29.11	43.20	<0.02	1.49	G1	S4	S4
1228+167	E	0.839	<31.42	31.06	45.66	<0.07	1.30	I1	K3	K3
1253-056	E	0.420	<32.02	29.39	44.11	<0.49	1.25	G1	G2	G2
1304+342	E	0.281	<30.38	29.36	44.43	<0.19	1.12	I1	K3	K3
1327+321	E	0.090	<30.69	28.98	43.58	<0.32	1.30	G1	S4	S4
1339+053	E	0.266	<31.09	30.20	44.7	<0.17	1.34	H4	M3	M3
1352+183	E	0.152	<29.85	30.18	44.94	<-0.06	1.24	I1	K3	K3
1352+184	E	0.977	<32.66	31.04	45.46	<0.30	1.37	I1	K3	K3
1357-024	E	0.416	<30.73	30.13	44.85	<0.11	1.25	I1	K3	K3
1401+098	E	0.43	32.19	30.77	45.15	0.26	1.38	I1	K3	K3
1403+546	E	0.082	<29.16	29.10	43.4	<0.01	1.41	H4	M3	M3
1415+252	E	1.057	<31.69	30.12	45.21	<0.29	1.11	G1	S4	S4
1415+254	E	0.560	<31.15	29.67	44.53	<0.28	1.20	G1	S4	S4
1416+254	E	0.674	<31.32	30.38	44.68	<0.17	1.41	G1	S4	S4
1430+054	E	0.202	<30.24	29.49	44.13	<0.14	1.28	G1	G2	G2
1439-053	E	0.620	<31.36	30.90	44.79	<0.09	1.57	G1	G2	G2
1519+279	E	0.230	<30.05	29.51	44.2	<0.10	1.26	H4	M3	M3
1525+155	E	0.230	31.76	29.83	44.51	0.36	1.27	G1	S4	S4
1526+286	E,Ton 236	0.450	<30.65	30.89	45.2	<-0.05	1.41	H4	M3	M3
1529+050	E	0.219	30.90	29.62	44.45	0.24	1.21	I1	K3	K3
1530+151	E	0.090	<29.50	28.72	43.60	<0.14	1.19	I1	K3	K3
1533+146	E	0.021	<28.39	28.27	42.12	<0.02	1.58	G1	S4	S4
1549+203	E,LB0905	0.250	<30.38	29.91	44.73	<0.09	1.21	G1	S4	S4
1553+159	E	1.324	<32.06	31.59	46.02	<0.09	1.36	G1	G2	G2
1557+272	E	0.065	<28.95	29.09	43.1	<0.03	1.53	H4	M3	M3
1602+241	E	0.087	<29.59	29.06	43.46	<0.10	1.37	I1	K3	K3
1604+158	E	0.357	<30.93	29.61	44.44	<0.24	1.21	G1	G2	G2

Table 3(c) - Continued

Object	Name	z	ℓ_{rc}	ℓ_o	ℓ_x	α_{ro}	α_{ox}	References r	o	x
1611-034	E	0.298	<30.82	30.01	44.21	<0.15	1.45	G1	G2	G2
1614+055	E	0.855	32.24	30.74	44.94	0.28	1.45	G1	G2	G2
1617+175	E,PG	0.116	<29.76	30.01	44.13	<-0.05	1.48	G1	S4	S4
1640+396	E	0.540	32.61	30.34	45.2	0.42	1.20	H4	M3	M3
1640+401	E	0.986	32.45	31.43	45.4	0.19	1.54	H4	M3	M3
1641+399	E	0.704	<32.35	31.23	45.2	<0.21	1.54	H4	M3	M3
1641+399	E	0.594	<32.20	30.04	44.9	<0.40	1.20	H4	M3	M3
1701+610	E	0.164	<30.06	29.70	43.7	<0.07	1.53	H4	M3	M3
1726+499	E	0.815	<31.19	30.37	45.3	<0.15	1.17	H4	M3	M3
1745+277	E	0.156	<30.17	29.06	43.57	<0.20	1.33	G1	S4	S4
1747+686	E	0.063	<29.01	29.05	43.63	<-0.01	1.31	I1	K3	K3
1847+335	E	0.509	<31.06	30.62	45.2	<0.08	1.31	H4	M3	M3
2041-310	E	0.434	<30.62	30.25	44.6	<0.07	1.39	H4	M3	M3
2124-149	E	0.057	<29.26	29.65	42.59	<-0.07	1.93	G1	G2	G2
2125-149	E	0.304	<30.65	29.83	44.12	<0.15	1.41	G1	G2	G2
2141+040	E	0.410	<30.87	29.71	44.45	<0.22	1.24	G1	S4	S4
2223-052	E	1.866	<32.99	31.65	45.85	<0.25	1.45	G1	S4	S4
2215-037	E	0.242	<30.70	29.96	44.5	<0.14	1.32	H4	M3	M3
2216-043	E	0.243	<30.10	29.47	44.1	<0.12	1.29	H4	M3	M3
2251-178	MR	0.068	29.14	29.08	43.32	0.11	1.43	I1	K3	K3
2344+184	E	0.138	29.91	29.96	43.5	<-0.01	1.71	H4	M3	M3
2348+199	E	0.043	29.24	28.41	42.68	0.15	1.42	G1	G2	G2
2355-329	E	0.071	<29.03	28.41	43.2	<0.12	1.23	H4	M3	M3

Table 4 : BL Lac Object Continuum Spectra

(a) Radio Selected BL Lac Objects

Object	Name	z	ℓ_{rc}	ℓ_o	ℓ_x	α_{ro}	α_{ox}	References r	o	x
0048-097	PKS	...	...	...	...	0.66	1.44	W1	H3	M1
0109+22	GC	...	...	...	...	0.50	1.59	P2	H3	O1
0118-272	PKS	...	...	...	...	0.59	1.37	L2	V3	L2
0212+73	S5	...	...	...	...	0.75	1.01	B1	B1	B1
0215+015	PKS	1.649	34.72	31.59	46.10	0.58	1.33	S6	H3	S1
0219+428	3CR 66A	0.444	33.70	31.43	45.08	0.42	1.66	U2	H3	S1
0235+164	AO	0.852	34.93	31.91	45.47	0.56	1.70	U2	H3	S1
0306+102	PKS	...	...	...	...	0.70	1.25	O2	H3	O1
0338-214	PKS	0.048	31.97	29.11	42.85	0.53	1.63	P2	P2	S1
0422+004	PKS	...	...	...	...	0.59	1.43	W1	H3	O1
0454-234	PKS	0.89	34.91	30.96	45.48	0.73	1.33	P2	P2	S1
0454+84	S5	...	...	...	...	0.61	1.57	B1	B1	B1
0521-365	PKS	0.055	33.09	29.51	43.80	0.66	1.42	K2	H3	S1
0528-250	PKS	2.77	35.67	32.58	46.88	0.57	1.41	P2	H3	S1
0537-441	PKS	0.894	35.18	31.98	45.66	0.60	1.65	P2	H3	S1
0716+71		...	...	...	...	0.32	1.80	B1	B1	B1
0735+178	PKS	0.424	34.24	31.64	45.08	0.48	1.74	U2	H3	S1
0754+100	OI 090	...	...	...	...	0.37	1.78	M1	H3	M1
0808+019	PKS	...	...	...	...	0.62	1.17	L2	H3	L2
0818-128	OJ 131	...	...	...	...	0.44	1.78	M1	H3	M1
0829+046	OJ 49	...	...	...	...	0.48	1.42	M1	H3	M1
0851+202	OJ 287	0.306	33.98	31.50	45.63	0.46	1.48	P2	H3	S1
1034-293	PKS	...	...	...	...	0.75	1.25	L1	H3	L1
1147+245	B2	...	...	...	...	0.55	1.59	L2	H3	L2
1215+303	B2	...	...	...	...	0.46	1.28	O2	H3	W6
1219+285	W Com	0.1	32.91	29.35	44.11	0.66	1.24	O3	H3	O1
1307+121	4C 12.46	...	...	...	...	0.77	1.27	J1	H3	M1
1308+326	B2	0.997	35.04	30.64	46.04	0.82	0.99	U2	H3	S1
1400+162	4C 16.39	0.244	32.61	30.23	44.46	0.44	1.44	W4	H3	S1
1413+135	PKS	0.26	33.55	28.89	44.08	0.87	1.07	P2	P2	S1
1424+240	PKS	...	...	...	...	0.52	1.31	L2	V1	L2
1514+197	PKS	...	...	...	...	0.70	>1.36	W4	H3	M1
1514-241	AP Lib	0.049	32.47	29.45	43.38	0.56	1.55	U2	H3	S1
1538+149	4C 14.60	...	...	...	...	0.56	1.60	L1	H3	L1
1727+502	IZw 186	0.055	31.31	29.11	44.40	0.41	1.03	W1	H3	S1
1749+096	4C 09.57	...	...	...	...	0.66	1.39	P2	H3	H1
1803+78	S5	...	...	...	...	0.66	1.37	B1	B1	B1
1807+698	3CR 371	0.051	32.14	29.78	43.30	0.44	1.71	P2	K2	S1
1921-293	OV 236	0.353	34.73	30.33	45.23	0.82	1.18	P2	P2	S1
2007+77	S5	...	...	...	...	0.63	1.42	B1	B1	B1
2131-021	4C-02.81	0.56	34.57	30.25	44.95	0.80	1.26	P2	H3	S1
2200+420	BL Lac	0.070	33.15	30.21	44.08	0.55	1.58	U2	H3	S1
2201+171	MC3	1.08	34.59	30.90	45.60	0.69	1.26	C4	H3	S1
2201+044	4C 04.77	0.028	31.00	28.50	42.70	0.47	1.45	W4	B2	S1
2223-055	3CR 446	1.404	35.39	31.38	46.88	0.75	0.98	U2	H3	S1
2233-148	PKS	...	...	...	...	0.79	1.09	L2	V1	L2
2251+158	3CR 454.3	0.859	35.55	31.69	46.11	0.72	1.37	P2	H3	S1
2254+074	OY 091	...	...	...	...	0.45	1.50	M1	H3	M1
2334+031	PKS	...	...	...	...	0.73	>1.16	O2	V1	M1

(b) X-ray Selected BL Lac Objects

Object	Name	z	ℓ_{rc}	ℓ_o	ℓ_x	α_{ro}	α_{ox}	References r	o	x
0317+182	E	0.19	31.42	29.39	45.20	0.38	0.83	G1	G2	G2
0323+022	H	0.147	31.85	30.15	45.50	0.32	1.01	F2	F2	F2
0414+009	H	...	...	...	...	0.39	0.96	U3	U3	U3
0548-322	PKS	0.069	31.67	29.56	44.95	0.39	0.99	S7	H3	S1
1101-232	4U, 2A	...	...	...	...	-0.33	1.29	S2	S2	W3
1101+384	Mkn 421	0.030	31.30	29.52	44.46	0.33	1.17	U2	H3	S1
1133+704	Mkn 180	0.046	31.35	29.32	44.30	0.38	1.15	W1	H3	S1
1207+397	E	0.59	31.98	30.03	45.50	0.36	1.00	S5	H3	S5
1218+304	2A	0.130	32.57	29.63	45.40	0.55	0.85	W5	H3	S1
1235+631	E	0.297	31.76	29.62	44.92	0.40	1.03	G1	G2	G2
1402+041	E	...	...	...	...	0.37	1.18	G1	S5	S5
1408+020	E	...	...	...	...	0.21	1.26	C1	C1	C1
1448+413	4U, 3A	...	...	...	...	-0.31	1.39	S3	S3	W3
1652+398	Mkn 501	0.034	31.80	29.56	44.71	0.42	1.08	U2	H3	S1
1704+607	E	...	...	...	...	0.37	1.06	C1	C1	C1
2155-304	PKS	0.117	32.21	30.56	46.00	0.31	1.10	U2	H3	S1

Table 5 : Other Compact Radio Source Continuum Spectra

Object	Name	Optical ID	m_v	α_{ro}	α_{ox}	References r	o	x
0026+346	B2	Red	21.4	0.97	>0.98	B3	B3	B3
0202+149	4C15.05	Red	21.9	1.08	0.76	L1	P2	L1
0221+06	4C06.11	QSO	19.5	0.82	0.94	P2	O1	O1
0406+121	PKS	IR,BL	22.0	0.97	0.93	L1	P2	L1
0500+019	PKS	Red	21.5	0.96	>0.92	L1	K5	L1
0506+101	PKS	Red	19.3	0.78	1.12	B3	V1	B3
0528+134	PKS	QSO	20.3	0.94	0.99	P2	P2	H1
0539-057	PKS	Red	19.7	0.84	>1.19	L1	K5	L1
0605-085	PKS	QSO	18.0	0.74	1.29	P2	P2	H1
0745+24	B2	QSO	18.5	0.75	1.18	P2	O1	O1
1117+146	4C14.41	QSO	20.0	0.88	>0.97	P2	P2	H1
1354-15	PKS	QSO	18.5	0.82	1.17	P2	P2	H1
1445-161	PKS	EF	>20	>0.85	<1.07	L1	L1	L1
1456+04	4C04.49	?	20.0	0.83	0.91	O2	O1	O1
1535+004	PKS	EF	>20	>0.85	...	L1	L1	L1
1548+056	4C05.64	QSO	18.0	0.72	1.24	P2	P2	H1
1600+335	PKS	Red	-23	-1.10	-0.71	L1	K5	L1
1823+56	4C56.27	QSO	18.5	0.76	1.07	P2	P2	H1
1936-155	PKS	BSO	20.5	0.89	>1.00	L1	V2	L1
2033+18	PKS	EF	>20	>0.74	...	C6	E1	H1
2128+048	PKS	EF	>20	>0.92	...	L1	L1	L1
2148+14	3C 437.1	Red	>22	>1.07	...	C6	K5	H1
2149+056	PKS	Red	20.6	0.86	>1.05	L1	K5	L1

References to Tables 3, 4, and 5

A1 - Arp, Sulentic and Tullio 1979.
B1 - Biermann *et al.* 1981.
B2 - Blumenthal, Keel, and Miller 1982.
B3 - Bregman *et al.* 1985.
B4 - Bregman 1984.
C1 - Chanan *et al.* 1982.
C2 - Condon *et al.* 1981a.
C3 - Condon *et al.* 1981b.
C4 - Condon and Jauncy 1974.
C5 - Cash and Snow 1980.
C6 - Cotton 1983.
E1 - Ekers 1969.
F1 - Feigelson, Isobe and Kembhavi 1984.
F2 - Feigelson *et al.* 1986.
G1 - Gioia *et al.* 1983.
G2 - Gioia *et al.* 1985.
H1 - Henriksen, Marshall, and Mushotzky 1984.
H2 - Hintzen, Ulvestad, and Owen 1983.
H3 - Hewitt and Burbidge 1980.
H4 - Helfand 1985, private communication.
I1 - This paper, Table 1a and 1b.
J1 - Jenkins, Pooley, and Riley 1977.
J2 - Junkkarinen, Marscher, and Burbidge 1982.
K1 - Ku, Helfand, and Lucy 1980.
K2 - Kuhr *et al.* 1981.
K3 - Kriss and Canizares 1982.
K4 - Kriss and Canizares 1985.
k5 - Kuhr 1986, private communication.
L1 - Ledden and O'Dell 1983.
L2 - Ledden and O'Dell 1985.
M1 - Madejski and Schwartz 1983.
M2 - Miley and Hartsuijker 1978.
M3 - Margon, Downes, and Chanan, 1985.
M4 - Marscher and Broderick 1981.
O1 - Owen, Helfand, and Spangler 1981.
O2 - Owen, Spangler and Cotton 1980.
O3 - Owen, Porcas, and Mufson 1978.
P1 - Pooley and Henbest 1974.
P2 - Perley 1982.
R1 - Riley and Pooley 1975.
R2 - Ryle and Elsmore 1973.
S1 - Schwartz and Ku 1983.
S2 - Schwartz *et al.* 1985.
S3 - Sramek and Weedman 1980.
S4 - Stocke *et al.* 1983.
S5 - Stocke *et al.* 1985.
S6 - Shimmins, Bolton, and Wall 1975.
S7 - Shimmins and Bolton 1974.
T1 - Tananbaum, Wardle, and Zamorani 1983.
U1 - Ulvestad *et al.* 1981.
U2 - Ulvestad, Johnston, and Weiler 1983.
U3 - Ulmer *et al.* 1983.
V1 - Veron-Cetty and Veron 1983.
V2 - Veron-Cetty and Veron 1984.
W1 - Wardle, Moore, and Angel 1984.
W2 - Worrall and Marshall 1984.
W3 - Wood *et al.* 1984.
W4 - Weiler and Johnston 1980.
W5 - Wilson *et al.* 1979.
W6 - Worrall *et al.* 1984.
Z1 - Zamorani *et al.* 1981.

Notes on individual objects for Tables 3, 4, and 5

3a. Radio Selected Quasars

0008+171 : 2.2 Jy at 178 MHz. $\alpha_{(1.8-5)}$=0.26.

0017+154 : Although the source is resolved in radio maps, the core is not detected by P1 and M2. The flux density of the west side lobe is used as the upper limit of the core.

0051+291 : $\alpha_{(2.7-5)}$=0.66

0056-001 : α_r from K2. Unresolved by Wills 1979.

0109+176 : The core at 20 cm is unresolved.

0119-046 : $\alpha_{(2.7-5)}$=0.37.

0133+207 : The core at 20 cm is unresolved by M2.

0134+329 : α_r from K2.

0135-247 : α_r from K2.

0229+341 : α_r from K2.

0237-027 : The redshift value from V2.

0237-233 : Unresolved by U1.

0312-770 : S(5GHz) from V1, and S(1.4GHz) from E1 for α_r.

0313+344 : Resolved but the core is not detected in radiomap of C3. The flux density of the fainter lobe (component B) is used as the upper limit.

0400+258 : α_r from K2.

0409+229 : α_r from P2.

0414-060 : $\alpha_{(2.7-5)}$= 0.78 from V2.

0424-131 : Unresolved by F1.

0438-436 : Unresolved by U1.

0440-003 : Partially resolved by U1.

0454-234 : The redshift value is from V2.

0518+165 : No map is available, the total flux is taken to the core upper limit.

0538+498 : No map is available, the total flux is taken to the core upper limit.

0607-157 : Unresolved by U2.

0710+118 : The map is available in J1 and M2.

0723-008 : The redshift value is from V2.

0740+380 : No map is available, the total flux is taken to be the core upper limit.

0758+144 : α_r from K3.

0802+104 : Unresolved by J1.

0805+046 : The core is unresolved at 1.4 GHz by F1.

0809+483 : Although the source is resolved, the core is not detected by P1. The lowest flux density given for one lobe is used as the upper limit of the core flux density.

0824+110 : $\alpha_{(2.7-5.0)}$=0.19 is from V2.

0830+112 : 1.4 GHz observation is not available.

0833+654 : The core is unresolved at 1.4 GHz.(M2)

0834-20 : $\alpha_{(2.7-5)}$=0.35 from V2. The redshift value from V2.

0835+580 : The core flux density at 20 cm is not available.

0837-120 : The core is resolved at 6 cm and 20 cm.

0838+133 : The core flux density at 20 cm is not available.

0850+140 : The core flux density at 20 cm is not available.

0855+143 : α_r from K3.

0906+431 : No map is availabe, the total flux is taken to be the upper limit. α_r is from K3.

0938+119 : No map is available, the total flux is taken to be the upper limit.

Notes on individual objects for Tables 3, 4, and 5 - Continued

0959-443 : The flux density, other than 5 GHz, is not available.
1004-217 : $\alpha_{(2.7-5)}$=0.0.
1023+067 : M2 gives the upper limit for the core.
1028+313 : The core is unresolved at 1.4 GHz.
1038+064 : $\alpha_{(2.7-5)}$=0.51.
1040+123 : The core flux density from J1 (5 GHz), and H2 (1.4 GHz).
1058+726 : Detected, but the map is needed.
1100+772 : The core flux density is the upper limit at 5 GHz . The source is unresolved at 1.4 GHz.
1111+408 : The maps are in M2 (5 GHz) and H2 (1.4 GHz). α_r=1.2.
1137+660 : The core is unresolved at 1.4 GHZ.
1157+014 : $\alpha_{(2.7-5)}$=0.33.
1219+04 : $\alpha_{(2.7-5)}$=0.18. The redshift value from V2.
1223+252 : The core is resolved at 5 GHz and 1.4 GHz.
1250+568 : No map is available, the total flux is taken to be the core upper limit.
1258+286 : The flux density at 1.4 GHz is not available.
1328+254 : No map is available, the total flux is taken to be the core upper limit.
1340+606 : The core flux density at 1.4 GHz is not available.
1413+135 : α_r from P2.
1422+202 : The core is unresolved at 1.4 GHz.
1435+248 : The core is unresolved by P1 (5 GHz) and H2 (1.4 GHz).
1442+101 : No map is available, the total flux is taken to be the core upper limit.
1458+718 : α_r from K2.
1502+106 : α_r from P2.
1522+155 : $\alpha_{(2.7-5)}$=0.38 is from V2.
1524+101 : The core is unresolved at 1.4 GHz by F1.
1525+227 : $\alpha_{(2.7-5)}$=0.66.
1545+210 : The core is unresolved at 1.4 GHz. (M2)
1548+114 : The core is resolved at 5 GHz and 1.4 GHz.
1555+332 : the core is resolved at 5 GHz and 1.4 GHz.
1556+335 : No map is available, the total flux is taken to be the core upper limit.
1606+289 : $\alpha_{(2.7-5)}$=1.12 from V2.
1622+238 : The core is unresolved at 1.4 GHz.
1623+269 : The core is unresolved at 1.4 GHz.
1632+391 : S(5 GHz)=376 mJy, S(1.4 GHz)=827 mJy. Both detected by our observation.
1704+608 : The core flux density at 1.4 GHz is not available.
1729+501 : The core is resolved at 5 GHz and 1.4 GHz.
1730-13 : $\alpha_{(2.7-5)}$= 0.24 and redshift value are from V2.
1756+237 : $\alpha_{(2.7-5)}$= 0.15.
1828+487 : α_r from K2.
1928+738 : α_r from P2.
2120+168 : The core is unresolved at 1.4 GHz.
2135-147 : The core is unresolved at 1.4 GHz by M2.
2141+175 : No map is available, the total flux is taken to be the core upper limit.
2230+114 : No map is available, the total flux is taken to be the core upper limit.
2251+113 : The core is unresolved at 1.4 GHz by F1.
2255+416 : α_r from K2.
2345-167 : No map is available, the total flux is taken to be the core upper limit.

3b. Optically Selecteced Quasars
0241+011 : The optical magnitudes are from A1. V(z=1.941)=19.6, V(z=0.599)=18.9, and V(z=1.411)=20.1.
0854+194 : Although this source has the radio name "OTL", we classify this as an optically selected quasar. This object is detected by our observation. S(5 GHz) = 1.8 mJy (Table 2a).

3c. X-ray Selected AGNs.
0038-015 : Extended radio source. The core flux density is 64 mJy.
0136+060 : Extended radio source. The core flux density is 2.9 mJy.
0809+481 : X-ray luminosity is possibly contaminated by a nearby G star.
0849+284 : The optical magnitude is at the observation limit (S4).
1415+252 : The optical magnitude is at the observation limit (S4).
1614+055 : Extended radio source. The core flux density is 5.0 mJy.

4a Radio Selected BL Lac Objects.
0521-365 : α_r=0.48.
1215+303 : Since Worrall *et al.*give S(1keV)=0.7±1.0 μJy, we used $S(2keV)$ =0.6 μJy as the averaged value.
1219+285 : Redshift is obtained from Weistrop *et al.* 1985.
1400+162 : α_r=0.44.
2223-055 : α_r=0.37.

4b. X-ray Selected BL Lac Objects.
0323+022 : Redshift is obtained from Fillipenko *et al.* 1986.
1101-232 : Since S2 gives only the radio flux density at 1.4 GHz, we assume f(5GHz) ~ f(1.4GHz).
1448+413 : Since S2 gives only the radio flux density at 1.4 GHz, we assume f(5GHz) ~ f(1.4GHz).

5. Other Compact Radio Sources.
0026+346 : Although it is reported at a 2.7 σ significance level in X-rays, we treat this object as undetected.
0500+019 : The optical magnitude is the red magnitude.
0529-057 : The optical magnitude is the red magnitude.
1600+335 : The optical magnitude is the red magnitude. Although it is reported at a 1.9 σ significance level in X-rays, we treat this object as undetected.
1936-155 : Although it is reported at a 2.4 σ significance level in X-rays, we treat this object as undetected.
2148+14 : The optical magnitude is red magnitude. Although it is reported at a 1.5 σ significance level in X-rays, we treat this object as undetected.
2149+056 : The optical magnitude is red magnitude.

Table 6a Correlations

Sample	Variables	Total no. objects	Censored objects			Significnat level of correlations		Plot no.
	x y		x	y	both	Cox (%)	BHK (%)	
Radio Selected	$\log(\ell_r)$-$\log(\ell_x)$	156	50	7	4	...	<0.01	1a
Quasars	$\log(\ell_o)$-$\log(\ell_x)$	156	0	11	0	<0.01	<0.01	2a
	$\log(\ell_o)$-$\log(\ell_r)$	156	0	54	0	<0.01	<0.01	3a
	α_{ro} - α_{ox}	156	50	7	4	<0.01	<0.01	4a
Optically	$\log(\ell_r)$-$\log(\ell_x)$	103	18	6	68	...	<0.01	1b
Selected	$\log(\ell_o)$-$\log(\ell_x)$	103	0	74	0	<0.01	<0.01	2b
Quasars	$\log(\ell_o)$-$\log(\ell_x)$	103	0	86	0	0.02	0.2	3b
	α_{ro} - α_{ox}	103	18	6	68	...	<0.01	4b
X-ray Selected	$\log(\ell_r)$-$\log(\ell_x)$	122	103	0	0	...	<0.01	1c
AGNs	$\log(\ell_o)$-$\log(\ell_x)$	122	0	0	0	<0.01	<0.01	2c
	$\log(\ell_o)$-$\log(\ell_r)$	122	0	103	0	<0.01	<0.01	3c
	α_{ro} - α_{ox}	122	103	0	0	...	52	4c
Radio Selected	$\log(\ell_r)$-$\log(\ell_x)$	24	0	0	0	<0.01	<0.01	1d
BL Lac Objects	$\log(\ell_o)$-$\log(\ell_x)$	24	0	0	0	<0.01	<0.01	2d
	$\log(\ell_o)$-$\log(\ell_r)$	24	0	0	0	<0.01	<0.01	3d
	α_{ro} - α_{ox}	49	0	2	0	...	<0.01	4d

X-ray Selected	$\log(\ell_r)-\log(\ell_x)$	10	0	0	0	2	3	1d
BL Lac Objects	$\log(\ell_o)-\log(\ell_x)$	10	0	0	0	0.03	0.3	2d
	$\log(\ell_o)-\log(\ell_r)$	10	0	0	0	0.7	0.7	3d
	$\alpha_{ro} - \alpha_{ox}$	16	0	0	0	4	2	4d
Compact Radio Sources	$\alpha_{ro} - \alpha_{ox}$	19	0	1	8	...	0.03	4e
Flat Spectral	$\log(\ell_r)-\log(\ell_x)$	66	0	2	0	<0.01	<0.01	...
Radio Quasars	$\log(\ell_o)-\log(\ell_x)$	66	0	2	0	<0.01	<0.01	...
	$\log(\ell_o)-\log(\ell_r)$	66	0	0	0	<0.01	<0.01	...
	$\alpha_{ro} - \alpha_{ox}$	66	0	2	0	<0.01	<0.01	...

Table 6b Linear Regressions

Sample	Variables	Total no. objects	Censored objects			Intercept Coeff. / Slope Coeff. / Standard Deviation	
	x y		x	y	both	EM	B-J
Radio Selected Quasars	$\log(\ell_r)$-$\log(\ell_x)$	156	50	7	4	29.0±...	
						0.48±0.06	
						...	
	$\log(\ell_o)$-$\log(\ell_x)$	156	0	11	0	23.9±1.6	23.8±...
						0.70±0.05	0.70±0.05
						0.47	0.45
	$\log(\ell_o)$-$\log(\ell_r)$	156	0	54	0	5.62±3.73	6.05±...
						0.91±0.12	0.89±0.12
						1.05	0.96
	α_{ro} - α_{ox}	156	50	7	4	...	
						-0.75±0.12	
						...	
Optically Selected Quasars	$\log(\ell_r)$-$\log(\ell_x)$	103	18	6	68	28.2± ...	
						0.51+0.15/-0.11	
						...	
	$\log(\ell_o)$-$\log(\ell_x)$	103	0	74	0	23.1±1.9	23.1± ...
						0.70±0.06	0.70±0.07
						0.50	0.48

	$\log(\ell_o)$-$\log(\ell_x)$	103	0	86	0	0.32±0.65 -0.68± ...
						0.97±0.21 1.01±0.27
						1.39 1.25
	α_{ro} - α_{ox}	103	18	4	68	...
						-0.60+0.04/-0.05
						...
X-ray Selected	$\log(\ell_r)$-$\log(\ell_x)$	122	103	0	0	...
AGNs						0.46+0.08/-0.06
						...
	$\log(\ell_o)$-$\log(\ell_x)$	122	0	0	0	18.2±1.4
						0.87±0.05
						0.43
	$\log(\ell_o)$-$\log(\ell_r)$	122	0	103	0	-34.5±12.1 ...
						2.08±0.40 ...
						2.42 ...
	α_{ro} - α_{ox}	122	103	0	0	...
						...
						...
Radio Selected	$\log(\ell_r)$-$\log(\ell_x)$	24	0	0	0	18.7±2.6
BL Lac Objects						0.77±0.08
						0.50
	$\log(\ell_o)$-$\log(\ell_x)$	24	0	0	0	17.8±3.3
						0.89±0.11
						0.59

	$\log(\ell_o)$-$\log(\ell_r)$	24	0	0	0	3.23±4.13	
						1.00±0.14	
						0.74	
	α_{ro} - α_{ox}	49	0	2	0	1.95±0.11	1.95±...
						-0.93±0.18	-0.93±0.19
						0.18	0.18
X-ray Selected BL Lac Objects	$\log(\ell_r)$-$\log(\ell_x)$	10	0	0	0	14.4±0.92	
						0.96±0.29	
						0.34	
	$\log(\ell_o)$-$\log(\ell_x)$	10	0	0	0	11.4±6.9	
						1.13±0.23	
						0.27	
	$\log(\ell_o)$-$\log(\ell_r)$	10	0	0	0	14.7±7.9	
						0.56±0.27	
						0.31	
	α_{ro} - α_{ox}	16	0	0	0	1.59±0.15	
						-1.40±0.41	
						0.11	
Compact Radio Sources	α_{ro} - α_{ox}	19	0	1	8	...	
						-0.97+0.23/-0.16	
						...	
Flat Spectral Radio Quasars	$\log(\ell_r)$-$\log(\ell_x)$	66	0	2	0	22.6±2.7	22.6±...
						0.67±0.06	0.67±0.08
						0.43	0.42
	$\log(\ell_o)$-$\log(\ell_x)$	66	0	2	0	24.2±2.0	24.0±...
						0.69±0.06	0.70±0.06
						0.42	0.39

$\log(\ell_o)-\log(\ell_r)$	66	0	0	0	11.5±2.7 0.74±0.01 0.58	
$\alpha_{ro} - \alpha_{ox}$	66	0	2	0	1.91±0.11 -0.92±0.17 0.16	1.98±... -0.91±0.15 0.15

Table 7 : Partial Rank Correlation Coefficient

Sample	Correlation Fixed variable	$\log(\ell_r)$-$\log(\ell_x)$ $\log(\ell_o)$	$\log(\ell_o)$-$\log(\ell_x)$ $\log(\ell_r)$	$\log(\ell_o)$-$\log(\ell_r)$ $\log(\ell_x)$
Radio QSOs		0.31	0.45	0.13
Optical QSOs		0.05	0.16	0.08
X-ray QSOs		0.07	0.64	0.07
Radio BL Lacs		0.56	0.45	0.34
X-ray BL Lacs		0.09	0.60	0.48

Table 8: Kaplan-Meier Mean and Standard Deviation of α_{ro} and α_{ox}

Data	$\langle\alpha_{ro}\rangle$	$\langle\alpha_{ox}\rangle$
Radio QSOs	0.64±0.01	1.43+0.02/-0.03
Optical QSOs	(0.49±0.02)[1]	1.65±0.03
X-ray AGNs	0.48+0.05/-0.06	1.39±0.02
Radio BL Lacs	0.62±0.02	1.46±0.03
X-ray BL Lacs	0.37±0.02	1.11±0.04
Compact Radio Sources	0.93±0.03	1.12±0.03
Flat Spectrum Radio	0.63±0.02	1.39+0.03/-0.04

Table 9a : Correlations between α_{ox} and r or $\log(\ell_o)$

Sample censored no. / total no.	r - α_{ox} Cox prob. (%)	r - α_{ox} Intercept Slope Stand. Dev.	$\log(\ell_o)$ - α_{ox} Cox prob. (%)	$\log(\ell_o)$ - α_{ox} Intercept Slope Stand. Dev.
Radio QSOs (11/156)	9.1	1.27±0.05 0.21±0.10 0.20	<0.01	-2.21±0.62 0.11±0.02 0.19
Optical QSOs (73/102)	<0.01	1.35±0.07 0.54±0.13 0.21	<0.01	-1.94±0.72 0.11±0.02 0.19
X-ray AGNs (0/123)	37	1.38±0.03 -0.13±0.09 0.17	0.13	-0.10±0.54 0.05±0.02 0.16
Radio BL Lacs (0/24)	34	1.47±0.08 -0.25±0.22 0.22	29	0.05±1.25 0.04±0.04 0.22
X-ray BL Lacs (0/10)	9.7	1.07±0.05 -0.39±0.32 0.10	85	0.00±2.72 0.03±0.09 0.11

Table 9b : Correlations among α_{ox}, Redshift, and Optical Luminosity

Data censored no. total no.	Cox's prob.(%) joint z only ℓ_o only	EM Intercept Slope for z Slope for ℓ_o Standard Deviation
Radio QSOs	P(tot)<0.01	1.16±0.03
11/156	P(z)<0.01	-0.73±0.15
	P(ℓ_o)<0.01	0.25±0.03
		0.17
Optical QSOs	P(tot)=0.01	1.56±0.06
73/102	P(z)=53	0.21±0.28
	P(ℓ_o)=42	0.07±0.06
		0.20
X-ray AGNs	P(tot)<0.01	1.20±0.02
0/123	P(z)<0.01	-1.29±0.13
	P(ℓ_o)<0.01	0.27±0.03
		0.13
Radio BL Lacs	P(tot)=0.01	1.10±0.06
0/24	P(z)=0.02	-1.39±0.26
	P(ℓ_o)=0.01	0.26±0.05
		0.15

X-ray BL Lacs	P(tot)=23	0.90±0.12
0/10	P(z)=11	-0.48±0.32
	$P(\ell_o)$=77	0.08±0.90
		0.15

Table 9c : Correlation among α_{ox}, Redshift, and X-ray Luminosity

Data censored no. total no.	Cox's prob.(%) Joint z only l_x only	EM Intercept Slope for z Slope for ℓ_x Standard Deviation
X-ray AGNs	P(tot)<0.01	4.53±0.58
0/123	P(z)<0.01	0.87±0.20
	P(ℓ_x)<0.01	-0.21±0.04
		0.15
BL Lacs	P(tot)=51	3.52±1.50
0/24	P(z)=76	0.47±0.53
	P(ℓ_x)=47	-0.14±0.10
		0.21
X-ray BL Lac	P(tot)=21	1.98±1.07
0/10	P(z)=23	-0.22±0.34
	P(ℓ_x)=45	-0.07±0.07
		0.10

Table 10a : Comparison of Radio Quasars and BL Lac Objects

Property	Mean and Standard Deviation	censored no. / total no.
Radio luminosity	QSO : $\langle \log(\ell_r) \rangle = 33.88 \pm 0.128$	(46/156)
	BL Lac: $\langle \log(\ell_r) \rangle = 33.81 \pm 0.280$	(0/24)
	Gehan test : P = 79%	
	Logrank test: P = 91%	
Optical luminosity	QSO : $\langle \log(\ell_o) \rangle = 31.26 \pm 0.06$	(0/156)
	BL Lac: $\langle \log(\ell_o) \rangle = 30.54 \pm 0.23$	(0/24)
	Gehan test : P = 0.8%	
	Logrank test: P = 0.01%	
X-ray luminosity	QSO : $\langle \log(\ell_x) \rangle = 45.63 \pm 0.06$	(11/156)
	BL Lac: $\langle \log(Lx) \rangle = 44.89 \pm 0.24$	(0/24)
	Gehan test : P = 0.6%	
	Logrank test: P = 0.01%	
α_{ro}	QSO : $\langle \alpha_{ro} \rangle = 0.64 \pm 0.01$	(46/156)
	BL Lac: $\langle \alpha_{ro} \rangle = 0.62 \pm 0.02$	(2/50)
	Gehan test : P = 20%	
	Logrank test: P = 14%	
α_{ox}	QSO : $\langle \alpha_{ox} \rangle = 1.43^{+0.02}_{-0.03}$	(11/156)
	BL Lac: $\langle \alpha_{ox} \rangle = 1.46 \pm 0.03$	(2/50)

Gehan test : P = 29%

Logrank test: P = 25%

Table 10b : Comparison of Radio Quasars and BL Lac Objects ($0.8<z<1.7$)

Property	Mean and Standard Deviation	censored no. / total no.
Redshift	QSO : $\langle z \rangle = 1.11 \pm 0.03$	(0/57)
	BL Lac: $\langle z \rangle = 1.08 \pm 0.10$	(0/8)
	Gehan test : P = 42%	
	Logrank test: P = 81%	
Radio luminosity	QSO : $\langle \log(\ell_r) \rangle = 34.40 \pm 0.12$	(16/57)
	BL Lac: $\langle \log(\ell_r) \rangle = 35.04 \pm 0.12$	(0/8)
	Gehan test : P = 3%	
	Logrank test: P = 0.6%	
Optical luminosity	QSO : $\langle \log(\ell_o) \rangle = 31.34 \pm 0.06$	(0/57)
	BL Lac: $\langle \log(\ell_o) \rangle = 31.38 \pm 0.18$	(0/8)
	Gehan test : P = 82%	
	Logrank test: P = 92%	
X-ray luminosity	QSO : $\langle \log(\ell_x) \rangle = 45.78 \pm 0.05$	(3/57)
	BL Lac: $\langle \log(\ell_x) \rangle = 45.92 \pm 0.17$	(0/8)
	Gehan test : P = 59%	
	Logrank test: P = 44%	
α_{ro}	QSO : $\langle \alpha_{ro} \rangle = 0.60 \pm 0.02$	(16/57)
	BL Lac: $\langle \alpha_{ro} \rangle = 0.69 \pm 0.03$	(0/8)

Gehan test : P = 8%

Logrank test: P = 3%

α_{ox}

QSO : $\langle\alpha_{ox}\rangle$ = 1.37±0.02 (3/57)

BL Lac: $\langle\alpha_{ox}\rangle$ = 1.39+0.08/-0.10 (0/8)

Gehan test : P = 73%

Logrank test: P = 60%

References

Arp, H., Sulentic, J. W., and De Tullio, G. 1979, *Ap. J.* **229**, 489.

Avni, Y. and Tananbaum, H. 1982, *Ap. J.R* (*Letters*), **262**, L17.

Avni, Y. and Tananbaum, H. 1986, *Ap. J.*, **305**, 83.

Biermann, P., Duerbeck, H., Eckart, A., Fricke, K., Johnston, K. J.,Kühr, H., Liebert, J., Pauliny-Toth, I. I. K., Schleicher, H., Stockman, H., Strittmatter, P. A., and Witzel, A. 1981, *Ap. J.* (*Letters*), **247**, L53.

Blandford, R. D. 1984 in *Active Galactic Nuclei*, ed. J. E. Dyson (Manchester: Manchester Univ. Pr.) P. 281.

Blumenthal, G. R., Keel, W. C., and Miller, J. S. 1982, *Ap. J.*, **257**, 499.

Borra, E. and Corriveau, G. 1984, *Ap. J.*, **276**, 449.

Braccesi, A., Formiggini, L., and Gabdkfi, E. 1970, *Astr. Ap.*, **5**, 264.

Bregman, J. N. 1984, *Ap. J.*, **276**, 423.

Bregman, J. N. Glassgold, A. E. Huggins, P. J., and Kinney, A. L. 1985, *Ap. J.*, **291**, 505.

Cash, W. and Snow, T. P. Jr. 1980, *Astr. Ap.* **91**, L7.

Chanan, G. A., Margon, B., Helfand, D. J., Downes, R. A., and Chence, D. 1982, *Ap. J.* (*Letters*), **261**, L31.

Condon, J. J., Condon, M. A., Jouncey, D. L., Smith, M. G., Turtle, A. J., and Wright, A. E. 1981*a*, *Ap. J.* **244**, 5.

Condon , J. J. and Dressel, L. L. 1978, *Ap. J.*, **221**, 456.

Condon, J. J. and Jauncy, D. L. 1974, *A. J.* **79**, 1220.

Condon, J. J., O'Dell, S. L., Puschell, J. J., and Stein, W. A. 1981*b*, *Ap. J.* (*Letters*), **246**, 624.

Cotton, W. D. 1983, *Ap. J.*, **271**, 51.

Cruz-Gonzalez, I. and Huchra, J. P. 1984, *A. J.*, **89**, 441.

Efron, B. 1984, *J. Am. Stat. Assoc.*, **79**, 791.

Ekers, J. A. (*ed.*) 1969, *Aust. Phys. Astr. Suppl.*, **7**, 1.

Filippenko, A. V., Djorgovski, S., Spinrad, H., and Sargent, W. L. W. 1986, *A. J.*, **91**, 49.

Feigelson, E. D. and Berg, C. J. 1983, *Ap. J.*, **269**, 400.

Feigelson, E. D., Bradt, H., McClintook, J., Remillard, R., Urry, C. M., Tapia, S., Geldzahler, B., Johnston, K., Romanishin, W., Wehinger, P. A., Wyckoff, S., Madejski, G., Schwartz, D. A., Thorstensen, J., and Schaefer, B. E. 1986, *Ap. J.*, **302**, 337.

Feigelson, E. D., Isobe, T., and Kembhavi, A. 1984, *A. J.*, **89**, 1464, (Paper I).

Feigelson ,E. D. and Nelson, P. I. 1985, *Ap. J.*, **293**, 192.

Franceschini, A., Gioia, I. M., and Maccacaro, T. 1986, *Preprint*.

Gioia, I. M., Feigelson, E. D., Maccacaro, T., Schild, R., and Zamorani, G. 1983, *Ap. J.*, **271**, 524.

Gioia, I. M., Maccacaro, T., Schild, R. E., Stocke, J. T., Leibert, J. W. Danziger, I. J., Kunth, D., and Lub, J. 1984, *Ap. J.*, **283**, 495.

Henriksen, M. J., Marshall, F. E., and Mushotzky, R. 1984, *Ap. J.*, **284**, 491.

Hewitt, A. and Burbidge, G. 1980, *Ap. J. Suppl.*, **43**, 57.

Hintzen, A., Ulvestad, J., and Owen, F. 1983, *A. J.*, **88**, 709.

Isobe, T., Feigelson, E. D., and Nelson, P. I. 1986, *Ap. J.*, **306**, 490.

Jenkins, C. J., Pooley, G. G., and Riley, J. M. 1977, *Mem. R. A. S.*, **84**, 61.

Johnson, H. L. 1966, *Ann. Rev. A. Ap.*, **4**, 193.

Junkkarinen, V. T., Marscher, A. P., and Burbidge, E. M. 1982 *A. J.*, **87**, 845.

Katgert, P., Thuan, T. X., and Windhorst, R. A. 1983, *Ap. J.*, **275**, 1.

Kembhavi, A. 1986, *IAU Symposium* 119 in press.

Kembhavi, A. and Fabian, A. C. 1982, *M. N. R. A. S.*, **198**, 921.

Kembhavi, A., Feigelson, E. D., and Singh, K. P. 1986, *M. N. R. A. S.*,

220,51, (Paper II).

Königl, A. 1981, *Ap. J.*, **243**, 700.

Kriss, G. A. and Canizares, C. R. 1982, *Ap. J.*,**261**, 51.

Kriss, G. A. and Canizares, C. R. 1985, *Ap. J.*, **297**, 177.

Ku, W. H.-M., Helfand, D. J., and Lucy, L. B. 1980, *Nature*, **288**, 323.

Kühr, H., Witzel, A., Pauliny-Toth, I. I. K., and Nauber, U. 1981, *A. A. Suppl.*, **45**, 367.

Lancaster, J. F. and Quade, D. 1985, *J. Am. Stat. Assoc.*, **80**, 393.

Ledden, J. E. and O'Dell, J. E. 1983, *Ap. J.*, **270**, 434.

Ledden, J. E. and O'Dell, J. E. 1985, *Ap. J.*, **298**, 630.

Maccacaro, T. and Gioia, I. M. 1983 in *IAU Symposium* 104, *Early Evolution of the Universe* and *Its Present Structure*, eds. G. O. Abell and G. Chincarini (Dordrecht: Reidel) P.7.

Maccacaro, T., Gioia, I. M., Maccagni, D., and Stocke, J. J. 1984, *Ap. J.* (*Letters*), **284**, L23.

Maccagni, D. and Tarenghi, M. 1981, *Space Sci. Rev.*, **30**, 55.

Madejski, G. M. and Schwartz, D. A. 1983, *Ap. J.*, **275**, 467.

Margon, B., Downes, R. A., and Chanan, G. A. 1985, *Ap. J. Suppl.*, **59**, 23.

Marscher, A. P. and Broderick, J. J. 1981, *Ap. J.*, **249**, 406.

Marshall, H. L., Avni, Y., Braccei, A., Huchra, J. P., Tananbaum, H., Zamorani, G., and Zitelli, V. 1984, *Ap. J.*, **283**, 180.

Marshall, H. L., Zamorani, G., Huchra, J. P., Braccesi, A., and Zitelli, V. 1983, *Ap. J.*, **269**, 42.

Miley, G. K. and Hartsuijker, A. P. 1978, *A. A. Suppl.*, **34**, 129.

Miller, L. 1984, in *VLBI* and *Compact Radio Sources*, eds. R. Fanti, *et al.* (Dordrecht: Reidel), P. 189.

Owen, F. N., Porcas, R. W., and Mufson, S. L. 1978, *A. J.*, **83**, 685.

Owen, F. N., Helfand, D. J., and Spangler, S. R. 1981, *Ap. J. (Letters)*, **250**, L55.

Owen, F. N. and Puschell, J. J. 1982, *A. J.*, **87**, 595.

Owen, F. N., Spangler, S. R., and Cotton, W. D. 1980, *Ap. J.*, **85**, 351.

Perley, R. A. 1982, *A. J.*, **87**, 859.

Pooley, G. G. and Henbest, S. N. 1974, *M. N. R. A. S.*, **169**, 477.

Reichert, G. A., Mason, K. O., Thorstensen, J. R., and Bowyer, S. 1982, *Ap. J.*, **260**, 437.

Riley, J. M. and Pooley, G. G. 1975, *Mem. R. A. S.*, **80**, 105.

Ryle, M. and Elsmore, B. 1973, *M. N. R. A. S.*, **164**, 223.

Schlosman, I., Shaham, J., and Shaviv, G. 1984, *Ap. J.*, **287**, 534.

Schmidt, M. 1968, *Ap. J.* **151**, 393.

Schmidt, M. and Green, R. F. 1986, *Ap. J.*, **305**, 68.

Schmitt, J. H. M. M. 1985, *Ap. J.*, **293**, 178.

Schwartz, D. A. and Ku, W. H.-M. 1983, *Ap. J.*, **266**, 459.

Schwartz, D. A., Roberts, W., Murray, S., Huchra, J., Remillard, R., Bradt, H., McCintock, J., Tuohy, I., Buckky, D., Tapia, S., Feigelson, E. D., and Schmelz, J. 1985, *B. A. A. S.*, **17**, 608.

Sen, P. K. 1968, *J. Am. Stat. Assoc.*,**63**, 1379.

Shimmins, A. J. and Bolton, J. G. 1974, *Aust. J. Phys. Astro. Suppl.*, **32**, 1.

Shimmins, A. J., Bolton, J. G., and Wall, J. V. 1975, *Aust. J. Phys. Astro. Suppl.*, **34**, 63.

Sramek, R. A. and Weedman, D. W. 1980, *Ap. J.*, **238**,435.

Stocke, J. J., Liebert, J., Gioia, I. M., Grrffiths, R. E., Maccacaro, T., Danziger, I. J., Kunth, D., and Lub, J. 1983, *Ap. J.*, **273**, 458.

Stocke, J. J., Liebert, J., Schmidt, G. D., Gioia, I. M., Maccacaro, T., Schild, R. E., Maccagni, D., and Arp, H. C. 1985, *Ap. J.*, **298**, 619.

Sulentic, J. W. 1986, *Ap. J.*, **304**, 617.

Tananbaum, H., Avni, Y., Green, R. F., Schmidt, M., and Zamorani, G. 1986, *Ap. J.*, **305**, 57.

Tananbaum, H., Wardle, J. F. C., and Zamorani, G. 1983, *Ap. J.*, **268**, 60.

Tucker, W. 1983, *Ap. J.*, **271**, 531.

Ulmer, M. P., Brown, R. L., Schwartz, D. A., Patterson, J., and Cruddace, R. G. 1983 *Ap. J.* (*Letters*), **270**, L1.

Ulvestad, J., Johnston, K., Perley, R., and Fomalont, E. 1981, *A. J.*, **86**, 1010.

Ulvestad, J. S., Johnston, K. J., and Weiler, K. W. 1983, *Ap. J.*, **266**, 18.

Ulvestad, J. S. and Wilson, A. S. 1984, *Ap. J.*, **285**, 439.

Véron-Cetty, M. P. and Véron, P. 1983, *A. A. Suppl.*, **53**, 219.

Véron-Cetty, M. P. and Véron, P. 1984, *E. S. O. Sci. Rep.*, **1**, 1.

Wardle, J. F. C., Moore, R. L., Angel, J. R. P. 1984, *Ap. J.*, **279**, 93.

Weiler, K. W. and Johnston, K. J. 1980, *M. N. R. A. S.*, **190**, 269.

Weistrop, D., Shaffer, D. B., Hintzen, P., and Romanishin, W. 1985, *Ap. J.*, **292**, 614.

Wills, D 1979, *Ap. J.*, **39**, 291.

Wilson, A. S., Ward, M. J., Axon, D. J., Elvis, M., and Meurs, E. J. A. 1979, *M. N. R. A. S.*, **187**, 109.

Wood, K. S., Meekins, J. F., Yentis, D. J., Smathers, H. W., McNutt, D. P., Byram, E. T., Chubb, T. A., and Friedman, H. 1984, *Ap. J. Suppl.*, **56**, 507.

Worrall, D. M. and Marshall, F. E. 1984 *Ap. J.*, **276**, 434.

Worrall, D. M., Puschell, J. J., Bruhweiler, F. C., Sitko, M. L., Stein, W. A., Aller, M. F., Aller, H. D., Hodge, P. E., Rudy, R. J., Miller, H. R., Wisniewski, W. Z., Cordova, F. A., and Mason, K. O. 1984, *Ap. J.*, **284**, 512.

Zamorani, G. 1982, *Ap. J.* (*Letters*), **260**, L31.

Zamorani, G. 1984, in *VLBI* and *Compact Radio Sources*, eds. R. Fanti *et al.* (Dordreht: Reidel), P. 85.

Zamorani, G., Henry, J. P., Maccacaro, T., Tananbaum, H., Soltan, A., Avni, Y., Liebert, J., Stocke, J., Strittmatter, P. D., Weymann, R. J., Smith, M. G., and Condon, J. J. 1981, *Ap. J.* **245**, 357.

Figure Captions

Figure 1(a) Plot of the 0.5-4.5 keV X-ray luminosity against the 5 GHz radio luminosity density of the radio selected quasars. The detected points are represented by circles and the upper limits are represented by bars in this figure and all following figures. The solid line in this and following two figures is the regression line $\log(\ell_x)=a+b\log(\ell_r)$ obtained by the application of the BHK method.

1(b) Plot of the 0.5-4.5 keV X-ray luminosity against the 5 GHz radio luminosity density of the optically selected quasars.

1(c) Plot of the 0.5-4.5 keV X-ray luminosity against the 5 GHz radio luminosity density of the X-ray selected AGNs.

1(d) Plot of the 0.5-4.5 keV X-ray luminosity against the 5 GHz radio luminosity density of the BL Lac objects. The radio selected BL Lac objects are represented by circles and the X-ay selected BL Lac objects are represented by boxes. The solid line is the regression for the radio selected BL Lac objects and the dashed line is the regression line for the X-ray selected BL Lacs. Both regression lines are assumed to have a form $\log(\ell_x)=a+b\log(\ell_r)$ and computed by a least square method.

Figure 2(a) Plot of the 0.5-4.5 keV X-ray luminosity against 2500 Å optical luminosity density of the radio selected quasars. The solid line in this and the following two figures is the regression line

$\log(\ell_x)=a+b\log(\ell_r)$ by the EM algorithm with normal distribution.

2(b) Plot of the 0.5-4.5 keV X-ray luminosity against 2500 Å optical luminosity density of the optically selected quasars.

2(c) Plot of the 0.5-4.5 keV X-ray luminosity against 2500 Å optical luminosity density of the X-ray selected AGNs.

2(d) Plot of the 0.5-4.5 keV X-ray luminosity against 2500 Å optical luminosity density of the BL Lac objects. The radio selected BL Lac objects are represented by circles and the X-ay selected BL Lac objects are represented by boxes. The solid line is the regression line for the radio selected BL Lac objects and the dashed line is the regression line for the X-ray selected BL Lacs.

Figure 3(a) Plot of the 5 GHz radio luminosity density against 2500 Å optical luminosity density of the radio selected quasars. The solid line here and in the following figures is the regression line $\log(\ell_r)=a+b\log(\ell_o)$ by the EM algorithm with the normal distribution.

3(b) Plot of the 5 GHz radio luminosity density against 2500 Å optical luminosity density of the optically selected quasars. The uncertainty of the intercept coefficient is relatively large (0.32 ± 0.65).

3(c) Plot of the 5 GHz radio luminosity density against 2500 Å optical luminosity density of the X-ray selected AGNs. The uncertainty of the intercept coefficient is relatively large (-34.5 ± 12.0).

3(d) Plot of the 5 GHz radio luminosity density against 2500 Å optical luminosity density of the BL Lac objects. The radio selected BL Lac objects are represented by circles and the X-ay selected BL Lac objects are represented by boxes. The solid line is the regression line for the radio selected BL Lac objects and the dashed line is the regression line for the X-ray selected BL Lacs.

Figure 4(a) Plot of the α_{ox} against the α_{ro} of the radio selected quasars. The solid line is the regression line $\alpha_{ox}=a+b\alpha_{ro}$ by the application the BHK method. The bars in this figure and following four figures represent lower limits.

4(b) Plot of the α_{ox} against the α_{ro} of the optically selected quasars. Because of the large uncertainty for the intercept here and below, we do not fit a regression line.

4(c) Plot of the α_{ox} against the α_{ro} of the X-ray AGNs.

4(d) Plot of the α_{ox} against the α_{ro} of the BL Lac objects. The radio selected BL Lac objects are represented by circles and the X-ay selected BL Lac objects are represented by boxes. The solid line

is the regression line for the radio selected BL Lac objects and the dashed line is the regression line for the X-ray selected BL Lac objects.

4(e) Plot of the α_{ox} against the α_{ro} of the compact radio sources. The arrow in this figure represents an upper limit.

Authors' Addresses

Eric D. Feigelson and Takashi Isobe

Department of Astronomy, The Pennsylvania State University, University Park, PA 16802.

Kulinder P. Singh and Ajit Kembhavi

Tata Institute of Fundamental Research, Homi Bhabha Road, Bombay 400 005, India.

Fig. 1

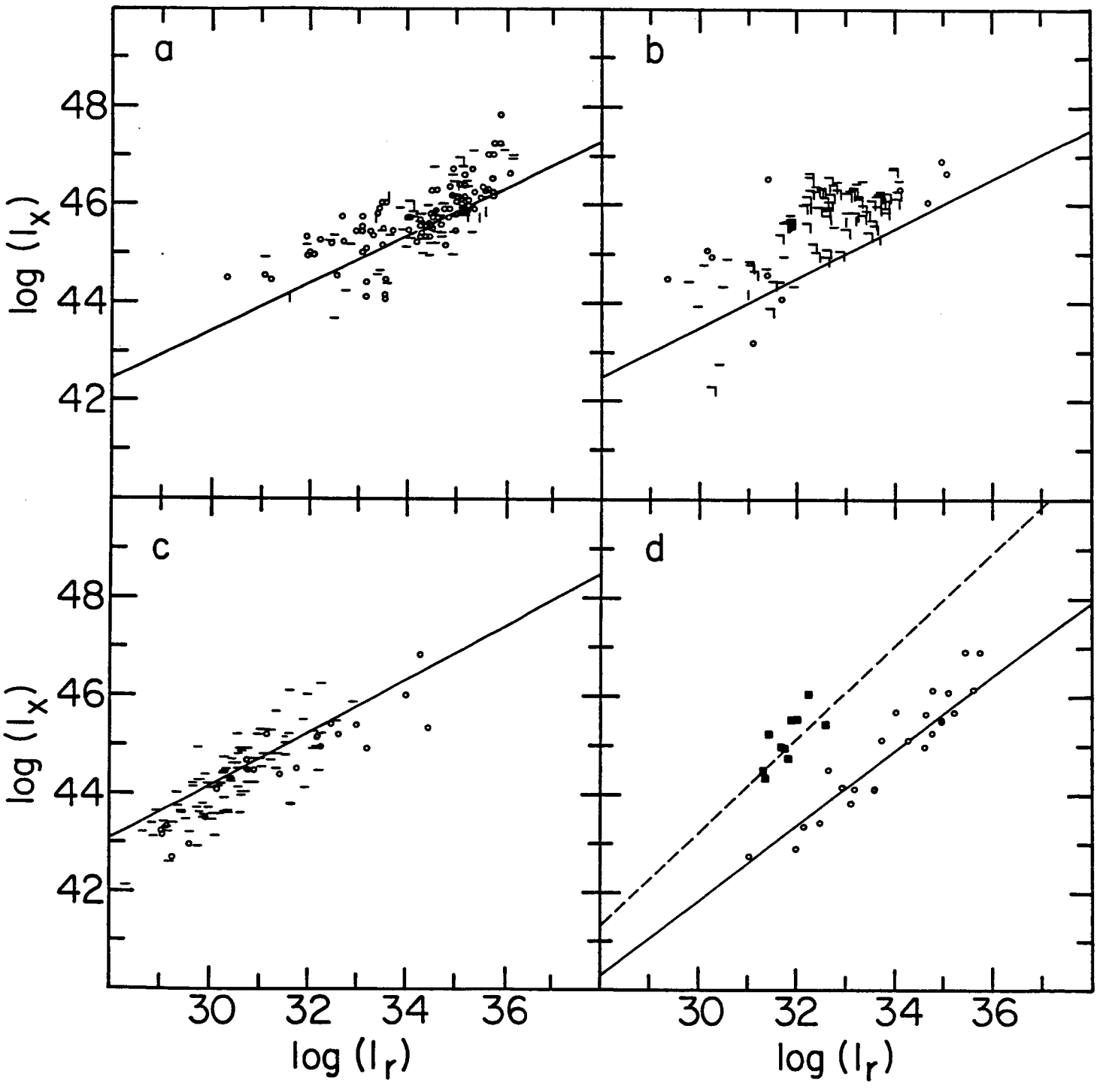

Fig. 2

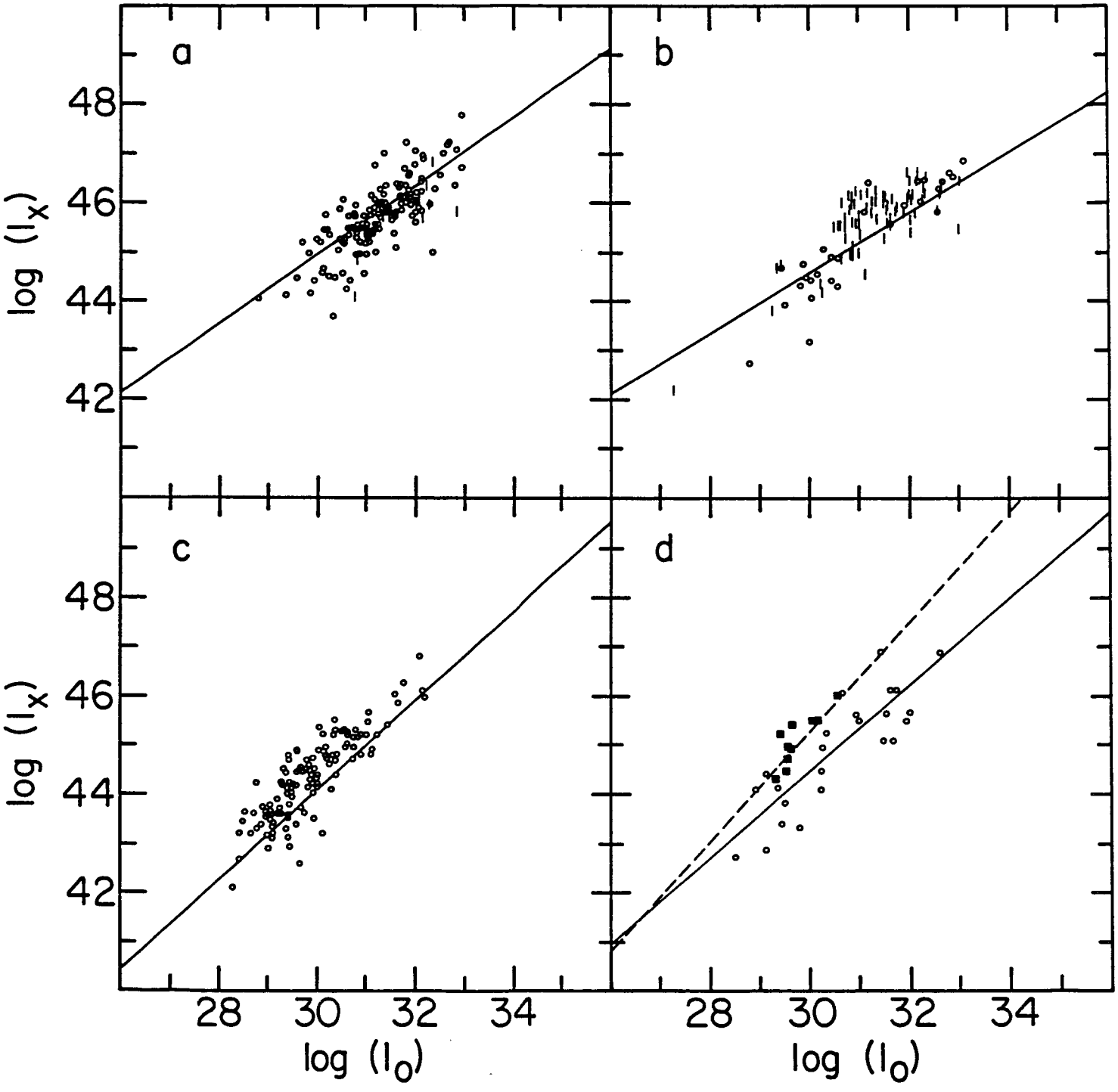

Fig. 3

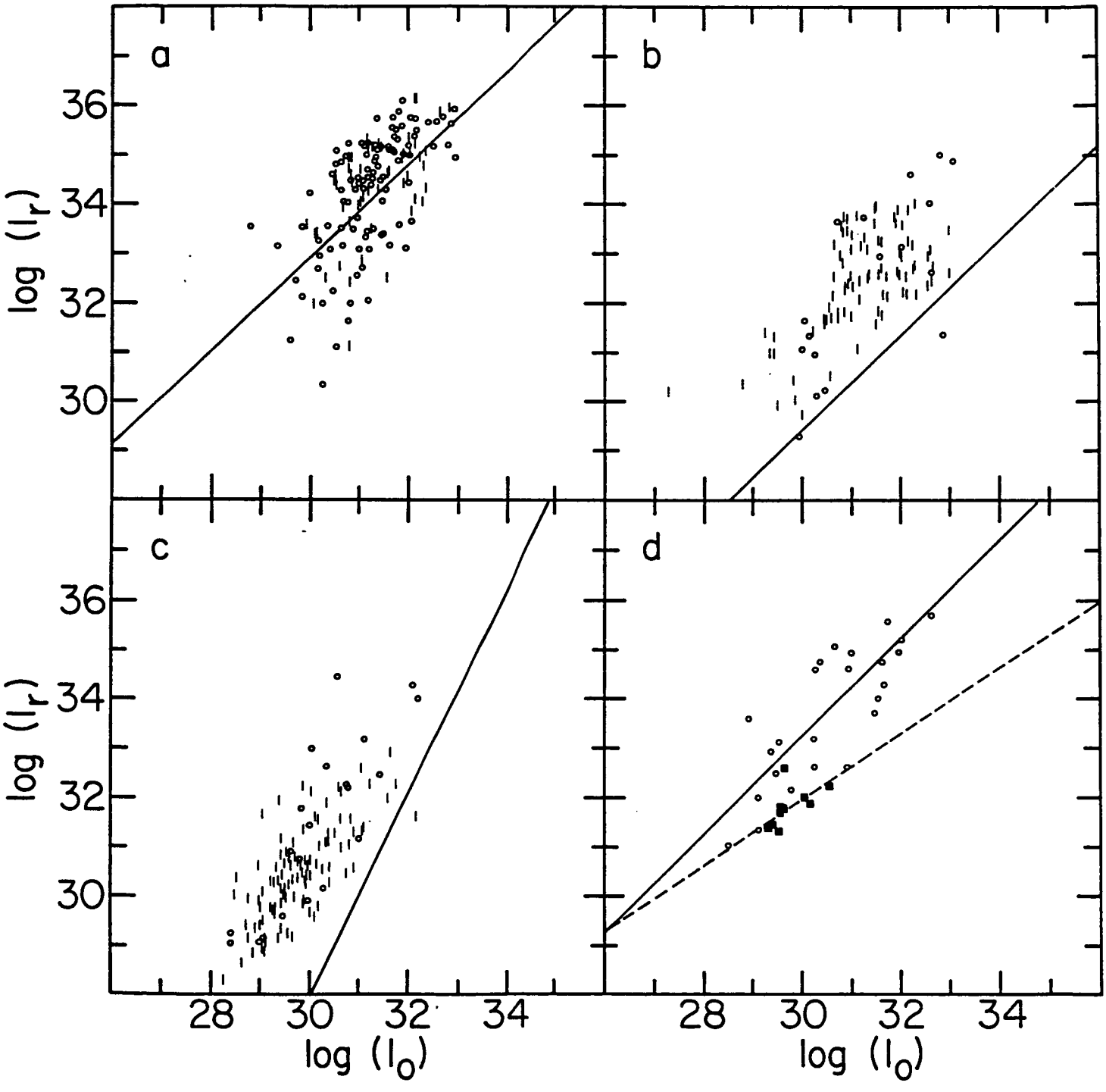

Fig. 4

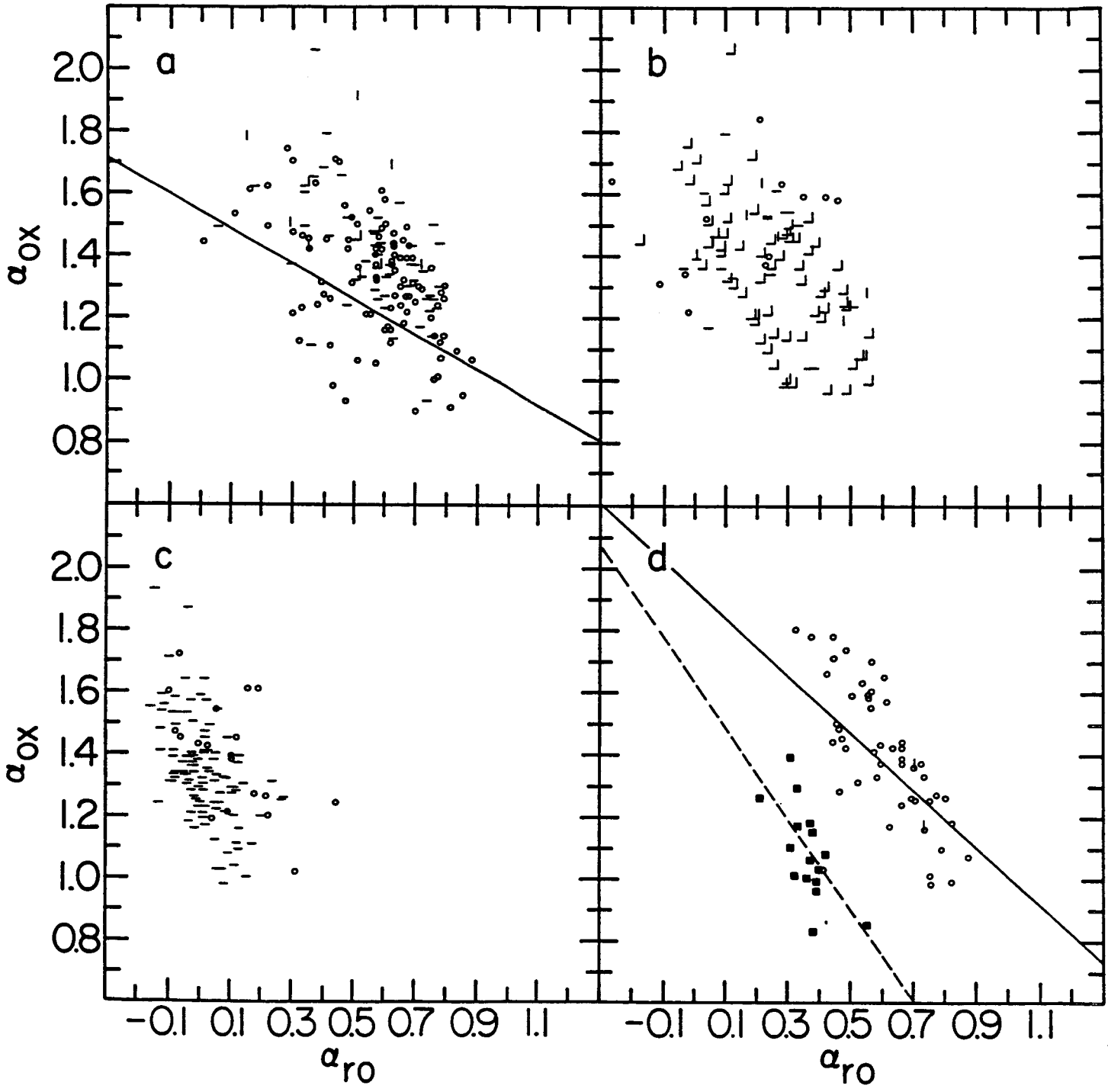

Fig. 4